Liquid treatment with a plasma jet surrounded by a gas shield : effect of the treated substrate and gas shield geometry on the plasma effluent conditions

Liquid treatment with a plasma jet surrounded by a gas shield: Effect of the treated substrate and gas shield geometry on the plasma effluent conditions

Pepijn Heirman[1], Ruben Verloy[1,2], Jana Baroen[1,2], Angela Privat-Maldonado[1,2], Evelien Smits[2] and Annemie Bogaerts[1]

[1] Research group PLASMANT, Department of Chemistry, University of Antwerp, Antwerp, Belgium
[2] Center for Oncological Research (CORE), IPPON, University of Antwerp, Antwerp, Belgium

Corresponding authors:
Pepijn Heirman, e-mail: pepijn.heirman@uantwerpen.be
Prof. Dr. Annemie Bogaerts, e-mail: annemie.bogaerts@uantwerpen.be

ABSTRACT

The treatment of a well plate by an atmospheric pressure plasma jet is common for *in vitro* plasma medicine research. Here, reactive species are largely produced through the mixing of the jet effluent with the surrounding atmosphere. This mixing can be influenced not only by the ambient conditions, but also by the geometry of the treated well. To limit this influence and control the atmosphere, a shielding gas is sometimes applied. However, the interplay between the gas shield and the well geometry has not been investigated. In this work, we developed a 2D-axisymmetric computational fluid dynamics (CFD) model of the kINPen plasma jet, to study the mixing of the jet effluent with the surrounding atmosphere, with and without gas shield. Our computational and experimental results show that the choice of well type can have a significant influence on the effluent conditions, as well as on the effectiveness of the gas shield. Furthermore, the geometry of the shielding gas device can substantially influence the mixing as well. Our results provide a deeper understanding of how the choice of setup geometry can influence the plasma treatment, even when all other operating parameters are unchanged.

1. INTRODUCTION

An atmospheric pressure plasma jet (APPJ) is a typical source of cold atmospheric plasma (CAP) used in plasma medicine research (1). The field of plasma medicine investigates the interaction between CAP and cells or tissue (2), and has shown promise for several applications, such as sterilization (2), wound healing (3, 4), and cancer treatment (5). Additionally, the use of APPJs is gaining attention in other fields, such as nitrogen fixation (6) and polymer treatment (7). An important example of an APPJ specifically developed for plasma medicine applications is the kINPen®. This medically certified plasma jet operates with argon as the feed gas and has been the subject of numerous studies (8-10).

Reactive oxygen and nitrogen species (RONS) produced by the plasma act as the major players in the biological effects induced by plasma treatment (11, 12). In a plasma jet that uses a noble gas as the feed gas,

like the kINPen, these reactive species can originate from two possible sources: either from impurities (or deliberate admixtures) in the feed gas (13, 14), or from mixing of the plasma effluent with the surrounding atmosphere (15). The latter makes plasma treatment with an APPJ susceptible to the ambient conditions during treatment, such as the relative humidity (16), which determines how much water can diffuse into the active plasma zone. This, in turn, plays a role in the RONS production and treatment reproducibility. To prevent this, a shielding gas device can be employed. First introduced in the context of plasma medicine by Reuter *et al.* (17), a gas shield induces a second, concentric gas flow that surrounds the jet and separates the plasma effluent from the surrounding air. The composition of the shielding gas can be controlled, thus allowing control over the gasses that are in contact with the plasma effluent. Since its introduction, the use of a gas shield with different gas compositions has been the subject of several studies. Although its effect on the RONS deposited in a treated liquid and its effect on treated cells has been studied (18, 19), its effect on RONS production in the gas phase is usually analyzed with operation of the free jet, i.e., without a substrate being treated. In fact, most diagnostic investigations of the kINPen plasma and its effluent have been performed on the free jet, without accounting for the effects caused by the presence of a substrate (8).

The treatment of biological tissue with an APPJ can be investigated *in vivo* (20-22), and some clinical trials have been reported (23, 24). However, most biomedical research is still performed *in vitro* (25, 26), where cell treatment is typically performed in well plates of varying sizes. Treatment of a well plate with a plasma jet, as opposed to e.g. a flat surface, inherently causes a backflow towards the jet outlet, of which the flow pattern logically depends on the well geometry. As such, this backflow may in turn influence the dynamics of both the jet effluent and, when used, the shielding gas. Moreover, cells *in vitro* are usually covered by a liquid layer such as cell medium. The gas flow over this liquid causes evaporation, which forms an additional source of water vapor that can affect the chemical pathways in the effluent, and thus the plasma treatment (27, 28).

The interaction between a plasma jet and a liquid forms a very complicated system, with many phenomena influencing each other (29). For this reason, simulations can be valuable for elucidating the different processes and their effect on the treatment (5). For the kINPen, and plasma jets in general, 0D models have been employed to investigate the chemical reaction pathways leading to RONS formation (30-33). To account for spatial phenomena, like convection and diffusion, multidimensional models have been developed to study e.g. mixing of the jet effluent with ambient species (34, 35) and the effects of e.g. flow rate (36) or molecular admixtures (13) on the RONS production. The influence of using a gas shield has also been investigated computationally (17, 37-39). Like gas phase diagnostics, however, these computational investigations are often performed for the free jet, without a substrate. Some computational efforts to investigate the interaction of a plasma jet with a liquid substrate have been reported. Lindsay *et al*. (40) presented a 2D axisymmetric model of a jet-like system above a petri dish, showing the importance of the induced convection in the liquid, while Verlackt *et al*. (41) developed a model with a more extensive chemistry set to investigate transport phenomena in a liquid-filled beaker treated by a plasma jet. Semenov *et al*. (42) presented a modelling study on the description of convection and diffusion in the system and at

the gas-liquid interface. In our previous work (43), we reported on a combined 0D/2D modelling approach to describe both the plasma chemistry and the transport of neutral species into the liquid. This model was applied to the kINPen above a well plate with buffered liquid water and investigated the stability of dissolved species after the treatment.

In the present work, we investigate how *in vitro* treatment with a plasma jet is affected by the choice of the used substrate (i.e. well size), as well as the interplay of this effect with a gas shield during treatment. For this purpose, we employ a computational 2D-axisymmetric model of the kINPen plasma jet above a liquid water surface, with and without a shielding gas device. Simulations are performed for various ambient conditions, such as temperature and relative humidity. This allows us to assess whether the gas shield is effective in eliminating variation caused by the ambient conditions for different setup geometries. Finally, attention is given to the geometry of the shielding gas device itself. Since the first report of a gas shield, different designs have been employed in different works (19, 35, 44). However, the possible effects of this change in geometry on, e.g., mixing of the shielding gas with the plasma jet effluent have rarely been addressed. Our simulations reveal that the design of the shielding gas device can have a substantial effect on the conditions in the plasma effluent and the effectiveness of the shielding.

2. METHODS

2.1 Computational methods

The description of the gas and liquid phase in the simulated system, i.e. a plasma jet above a well plate containing a liquid, is based on the modelling approach presented in (43). Here, we constructed the 2D-axisymmetric fluid dynamics model with COMSOL Multiphysics (version 6.0) (45). Figure 1 shows the simulated geometry. The plasma jet geometry is based on that of the kINPen, while the shielding gas device is based on a commercially available gas shield made by Neoplas GmbH specifically for the kINPen. The dimensions of the treated well in Figure 1 are those of a 24-well plate containing 1 mL of liquid, though different well sizes are used throughout the paper. Because of the impinging gas from the plasma jet, the liquid surface is deformed, causing a dimple of which the shape and depth depend on the treatment setup (46). The shape of the gas-liquid interface in our model is therefore based on observations made in our lab for the same setup geometry. Note that we treat the liquid surface in the model as stationary, and oscillations of the surface over time, as present in reality, are not yet accounted for. However, as we focus mainly on the effect of the substrate geometry on the gas phase dynamics, this assumption will not significantly influence our results. The distance between the jet nozzle and the liquid surface (in its original state) is 20 mm. We use a gas flow rate of 2 standard liters per minute (SLM) for the jet, and 4 SLM for the gas shield (when applied). We selected these conditions to make sure that, in the experiments performed with this geometry, there would be no liquid splashing out of the well, and the jet would operate in a non-touching regime, i.e. no direct discharge onto the liquid occurs. Both phenomena would significantly complicate the modelling description.

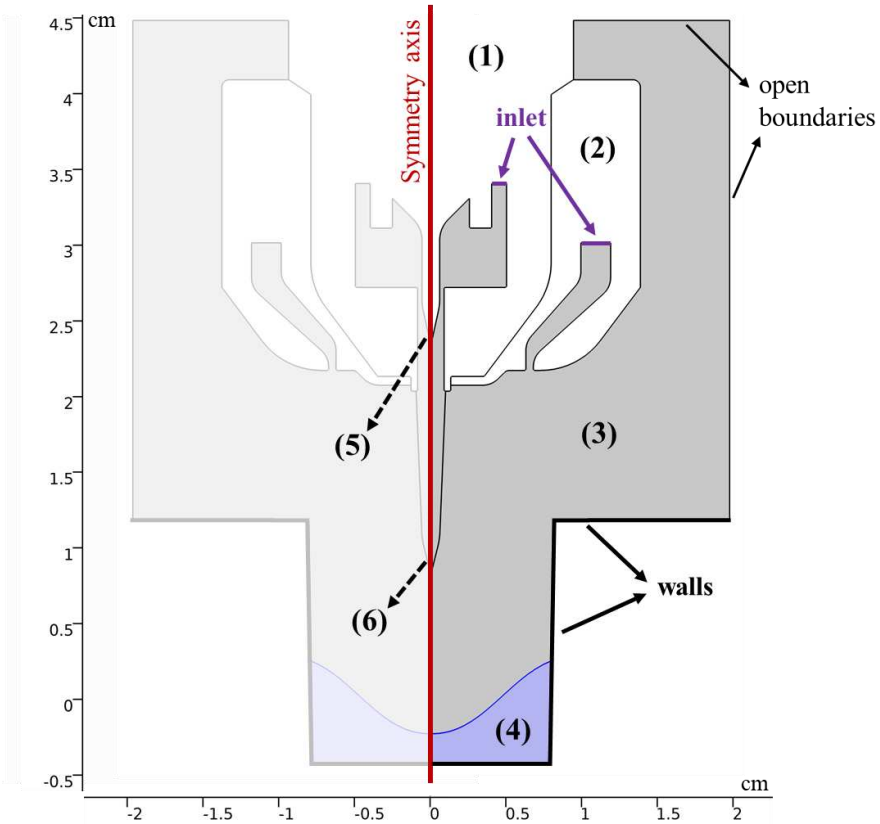

Figure 1 General model geometry. The geometry components are (1) the plasma jet, (2) the shield gas device, (3) gas phase and (4) liquid phase. The pin-electrode (5) and plasma plume (6) are also indicated. The boundary conditions applied at the edges of the model are indicated. As the geometry is 2D axisymmetric, only the right part is simulated by the model, with the symmetry axis indicated in red.

The plasma discharge itself is not simulated by the model. Instead, we study the species that typically lead to RONS formation in this system, i.e. the surrounding O_2, N_2 and H_2O, and their mixing with the feed gas from the jet. In this way, we hope to provide a deeper understanding of how the choice of setup geometry, like the treated well and the use of a gas shield, can influence the treatment even when all further operating parameters (which define the plasma discharge) are unchanged. The modelling approach is as follows: first, we calculate the stationary state of the flow field in the system. Using this stationary flow field as the input, we simulate the temperature and transport of species in the system in a time-dependent manner, for a treatment of 10 seconds. These simulations are performed for different geometries, of both gas shield and well plate, to elucidate their effect on the plasma jet effluent conditions.

2.1.1 Stationary calculation of the fluid flow

The flow field in the system is calculated by solving the time-independent, incompressible Navier-Stokes equations:

$$\rho \nabla \cdot \vec{u} = 0$$

$$\rho(\vec{u}\cdot\nabla)\vec{u} = \nabla\cdot[-p\mathbf{I}+\mathbf{K}]$$

With ρ the density (kg/m³), $\vec{u}$ the velocity vector (m/s) and p the pressure (Pa). **I** is the identity matrix, while **K** is the viscous stress tensor (Pa). When applying a gas flow rate of 2 SLM through the jet, the jet is in a turbulent regime (8). Therefore, we employed Menter's shear stress transport (SST) turbulence model (47) as implemented in the COMSOL CFD module.

Walls are treated with the no-slip boundary condition. At the open boundaries, a pressure of 1 atm is prescribed as a normal stress, while at the inlet of both the jet and the gas shield the inflow is prescribed as a fully developed flow profile. Finally, the gas-liquid interface is treated as a slip wall, by implementing a no-penetration boundary condition, as in reality the flowing gas sets the liquid in motion.

2.1.2 Time-dependent calculation of heat transfer and species transport

We calculated the temperature in the gas and liquid phase by solving the conservation of energy:

$$\rho C_p\frac{\partial T}{\partial t}+\nabla\cdot\vec{q}+\rho C_p\vec{u}\cdot\nabla T = Q$$

Where C_p is the heat capacity at constant pressure, T is the absolute temperature and $\vec{q}=-k\nabla T$ is the conductive heat flux, with k the thermal conductivity. Q represents additional heat sources like, in this model, viscous dissipation and heat loss due to water evaporation.

The transport of chemical species is calculated by solving the continuity equation:

$$\rho\frac{\partial n_i}{\partial t}+\nabla\cdot\vec{J}_i+\rho(\vec{u}\cdot\nabla)n_i = R_i$$

Here, n_i is the number density of species i, while $\vec{J}_i$ is its diffusive flux. R_i represents the net production or consumption of chemical species (equal to zero in case no chemical reactions are included). The continuity equation is solved for each species, except argon, of which the density is determined through the fact that the sum of all mass fractions must be equal to 1.

The diffusive flux is defined as:

$$\vec{J}_i = -D_{m,i}\nabla n_i - D_{T,i}\nabla n_i$$
$$with\ D_{T,i} = \frac{\mu_T}{\rho\cdot Sc_T}$$

Where $D_{m,i}$ is the mixture-averaged diffusion coefficient (48). $D_{T,i}$ is the eddy diffusivity; this additional diffusive flux accounts for the turbulent mixing by eddies that are not resolved by the turbulence model. $D_{T,i}$ depends on the turbulent viscosity μ_T, and on the turbulent Schmidt number, calculated by COMSOL based on (49). The binary diffusion coefficients used to determine $D_{m,i}$ are calculated within the model as described in (50), using tabulated data from (51). Other species-specific parameters C_p and k are also calculated within the model, as described in (52) and (53), respectively.

At the jet inlet, argon enters the domain, containing impurities (1 ppm O_2, 4 ppm N_2, 3 ppm H_2O (32, 43)). The temperature of the gas flowing into the system via this inlet is set to 327K as in (43). The gas shield inlet supplies dry air (79% N_2, 21% O_2) into the system, while at the open boundaries we specify a constant concentration of N_2, O_2, and H_2O equal to the initial conditions in the gas phase, i.e. humid air with a H_2O concentration that depends on the specified relative humidity and temperature. The temperature at both the gas shield inlet and the open boundaries is set to the initial ambient temperature, taken to be 293 K in the general case, but (when indicated) varied between 283 K and 303 K for different simulations. Walls are treated as thermally insulating, with a no penetration boundary condition for the chemical species. At the gas-liquid interface, water evaporation is accounted for with a flux that keeps the water density at the interface in line with the vapor pressure of water, which is in turn calculated via Antoine's law. Evaporative cooling, i.e. the heat loss at the liquid interface due to the evaporation of water, is implemented by prescribing a loss of heat at the interface as follows:

$$\mathrm{Q_{water\ evap}} = \mathrm{J_{H_2O}} \cdot \mathrm{H_{vap}}$$

With J the molar flux of water due to evaporation and H the latent heat of evaporation (for water = 2260 kJ/kg). Note that in our previous work (43), we confirmed the occurrence of this evaporative cooling experimentally, and implemented a correction factor to prevent large overestimation of the evaporative cooling at the gas-liquid interface in the model. In the present work, this correction factor is no longer needed. Briefly, the earlier overestimation stemmed from assuming $\mathrm{J_{H_2O}} = \mathrm{J_{z,H_2O}}$, i.e. the total axial flux of H_2O at the interface, as described in (40), which is an overestimation for a non-flat surface due to the large contribution of fluid flow in the axial direction.

Transport of chemical species other than H_2O over the gas-liquid interface is implemented with a flux governed by Henry's law:

$$\mathrm{c_{i,aq}} = \mathrm{H_i} \cdot \mathrm{RT} \cdot \mathrm{c_{i,g}}$$

Where $\mathrm{c_{i,aq}}$ and $\mathrm{c_{i,g}}$ are the concentrations of species i in the liquid and gas phase, respectively, and $\mathrm{H_i}$ is the temperature dependent Henry's constant (54).

2.2 Experimental methods

We performed experiments with the kINPen® MED to validate the computational results, using the same setup geometry as in the simulations, i.e. 2 SLM argon flow rate with a 20 mm gap between the kINPen nozzle and the liquid surface. The treatment time was 60 seconds in all experiments. Afterwards, deionized water was added to counter evaporation. Specifically, we compared the liquid volume in the different well types before and after treatment, showing that the treatment caused the evaporation of up to 2% of the liquid during the applied treatment time.

2.2.1 Determination of RONS in the treated liquid

Concentrations of long-lived RONS (H_2O_2, HNO_2 and HNO_3) were determined after treatment of a 12-, 24-, 48-, and 96-well plate (respectively 665180, Greiner; 10062-896, Avantor; 677180, Greiner and 655180, Greiner), containing 2 mL, 1 mL, 0.5 mL and 0.1 mL phosphate-buffered saline (PBS) per well, respectively. These volumes are typically used in experiments, as e.g. outlined in the standardized protocol by Tornin *et al.* (55), and correspond to solution depths of ca. 0.5 cm for the 12-, 24- and 48-well plates, and ca. 0.3 cm for the 96-well plate. Experiments were performed on three separate days, with three technical replicates each. Quantification of hydrogen peroxide in plasma-treated PBS (pPBS) was performed with the Fluorometric Hydrogen Peroxide Assay Kit from Sigma-Aldrich (MAK165-1KT), according to the supplier's instructions. The samples were diluted according to a 1:100 ratio in untreated PBS. The fluorescence intensity was measured at an excitation wavelength of 540 nm and an emission wavelength of 590 nm with the Tecan Spark Cyto 600. A standard curve was used to determine the concentration.

For nitrate and nitrite, quantification in pPBS was done with the Nitrate/Nitrite Colorimetric Assay Kit from Cayman Chemical (780001), according to the supplier's instructions. The samples were not diluted, except for the samples treated in a 96 well, which were diluted according to a 1:10 ratio in untreated PBS. The absorbance was measured at 540-550 nm with the Tecan Spark Cyto 600. Calibration curves were used to determine the concentrations.

2.2.2 Cell experiments

The human cancer cell line A375 (melanoma, ATCC®) was used in this study to determine the effect of the treatment on the cell viability. Cancer cells were cultured in Dulbecco's Modified Eagle Medium (DMEM, 10938025, Gibco) supplemented with 10 % fetal bovine serum (FBS, Gibco), 100 U/mL penicillin, 100 µg/mL streptomycin (15140122, Gibco) and 4 mM L-glutamine. The kINPen® MED was used to treat 2D monolayers of 96 000 A375 cells per well in a 24-flat well plate (10062-896, Avantor) with or without gas shield. The plasma setup was controlled by an automated stage using the program WinPC-NC. Hoechst (200nM, 62249, Life Technologies) and Cytotox Green (60 nM, 4633, Essen Bioscience) were added to measure both confluence and cell death with fluorescence imaging at 4h, 24h, and 72h. Experiments were performed on three separate days, with three technical replicates each.

3. RESULTS AND DISCUSSION

3.1 General modelling case

As the general case in our investigation, we chose the treatment of a 24-well plate containing 1 mL of liquid. Figure 2A shows the calculated stationary flow field in the gas phase, both without and with the gas shield (left vs right panel). As expected, the gas flow out of the shielding gas device completely envelopes the plasma effluent. As shown previously (43), without a gas shield the argon flow from the jet quickly displaces the gas that was initially in the well. This does not mean that the well becomes completely devoid of air; the vortex created in the well traps some of the surrounding air and mixes it with the effluent, keeping e.g. the

N_2 density in the well around 1.8 x10^{17} cm^{-3}. Adding a gas shield provides a constant inflow of air into the well, keeping the concentrations of O_2 and N_2 much higher, as shown in Figure 2B.

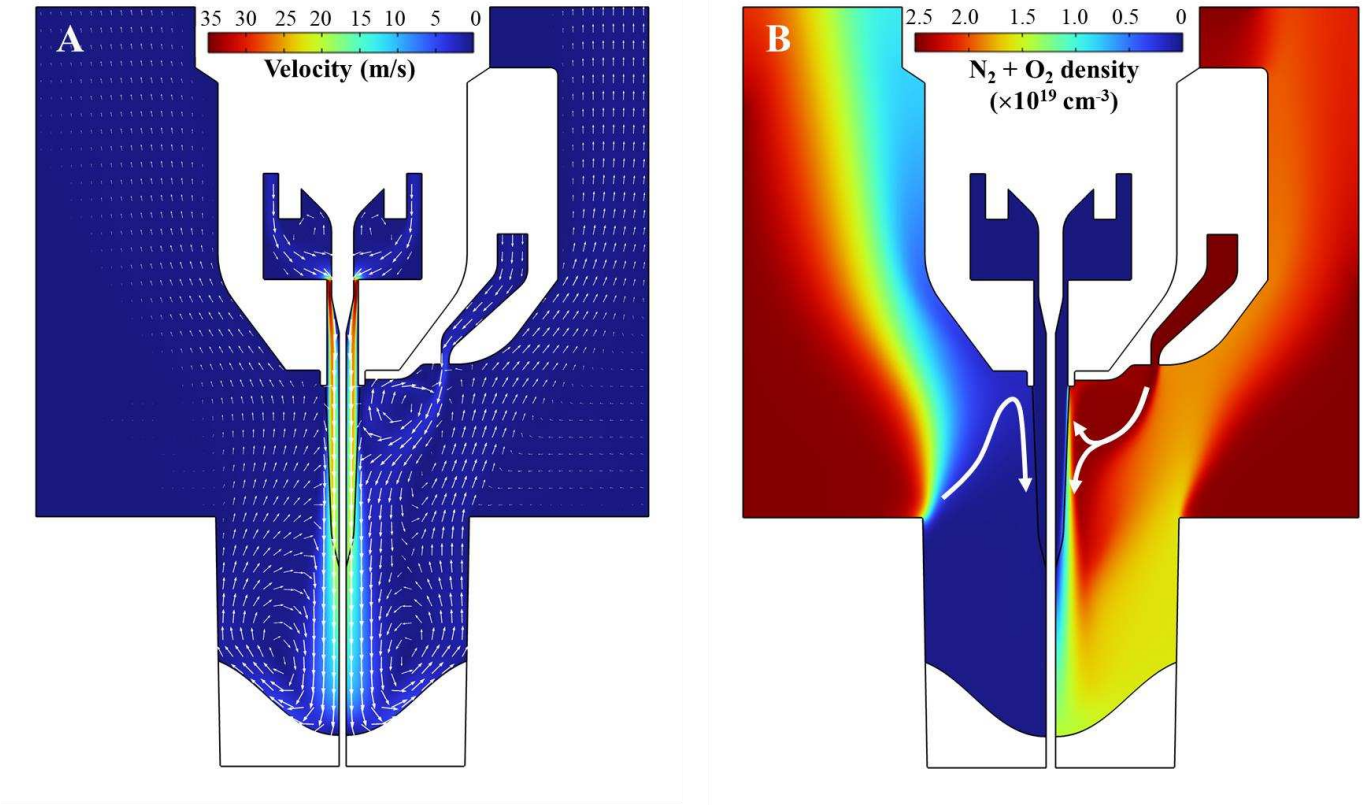

Figure 2 Calculated flow field (A) and air density (B) for the treatment of a 24-well plate, without (left panels) and with (right panels) gas shield. In (A), white arrows represent the flow field vectors, while in (B) they represent the main paths through which air mixes with the jet effluent.

3.1.1 N_2/O_2 in the plasma effluent

The kINPen produces a plasma plume of around 10 mm starting from the outlet of the jet nozzle. In this region, ambient species N_2, O_2 and H_2O are converted by electron impact reactions or reactions with excited Ar atoms into the primary reactive species that drive the RONS formation in the effluent (56). For this reason, we are most interested in the conditions in the immediate effluent of the jet, resulting from mixing of the plasma effluent with the ambient. Because of the high velocity of the gas flow exiting the jet, axial convection is the dominant transport mechanism over radial diffusion, even when turbulent mixing is taken into account. We can thus expect strong radial concentration gradients in this region. To obtain a picture of the entire effluent as opposed to, e.g., only the very center on the symmetry axis, we focus on the conditions at five different radial positions spanning the entire width of the jet nozzle. Figure 3A depicts the N_2 number density at these five radial positions, as a function of distance from the pin electrode. O_2 is not depicted here, but behaves in the same way as N_2, with absolute values four times lower, reflecting the N_2/O_2 ratio

in air. Near the edge of the jet effluent, at r = 0.75 mm, the N_2 number density rises very steeply immediately when the gas exits the jet nozzle (see first vertical dotted line). The ambient N_2 however only reaches the center of the effluent near the end of the plasma plume (second vertical dotted line). The number density does reach the same level over the entire width of the effluent before the gas flow reaches the liquid surface.

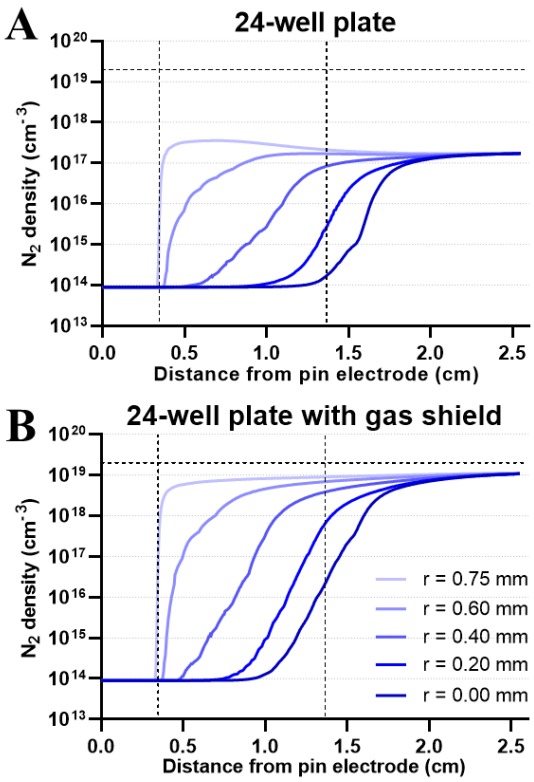

Figure 3 Calculated N_2 number density in the jet effluent without (A) and with (B) a shielding gas. The first (x = 0.35 cm) and second (x = 1.35 cm) vertical dotted lines indicate the jet nozzle and the end of the plasma plume, respectively, while the horizontal dotted line indicates the number density in the surrounding air (1 atm and 293 K).

With a shielding gas (Figure 3B), we can see the same qualitative behavior, but the gas shield significantly increases the absolute number densities of N_2 (and by extension, O_2) in the effluent. It is not surprising that the addition of a gas shield causes an increase of the number density of these species, especially near the edge of the jet effluent. However, even in the core plasma region the difference reaches up to two orders of magnitude, depending on the axial position. In diagnostic investigations of the kINPen, a gas shield is sometimes used not to exclude influence from the surrounding atmosphere, but to simulate the presence of a surrounding atmosphere of known composition (16), or to provide a surrounding atmosphere when directing the jet into a closed-off chamber for e.g. FTIR measurements (31, 57, 58). Our simulations reveal that mixing of the jet effluent with the gas surrounding it is significantly enhanced in the entire plasma effluent, when that surrounding gas originates from a gas shield as opposed to the ambient atmosphere. This means that caution must be taken when diagnostics in the presence of a gas shield are compared to

experiments without a gas shield, as they do not entail the same (quantitative) conditions in the active plasma zone.

3.1.2 H_2O in the plasma effluent

The main incentive to employ a gas shield is to limit the variation caused by different atmospheric conditions. The concentration of water in the atmosphere depends on the temperature and relative humidity. Hence, unlike O_2 or N_2, the amount of H_2O that mixes with the kINPen effluent can change from day to day, irrespective of the setup. The presence of H_2O substantially influences the CAP chemistry and can change the biological effects of CAP treatment (16, 59). Figure 4A and B illustrate the mixing of ambient H_2O with the plasma jet effluent in the same way as plotted for N_2 in Figure 3, i.e., for different radial positions. In addition, to assess the efficacy of the gas shield in eliminating variation caused by the surrounding humidity, we performed these simulations for three different ambient temperatures (283 K, 293 K, and 303 K) and for three different ambient relative humidities (0%, 50% and 100%), yielding a total of nine conditions. The results are shown in Figure 4C and D. For clarity, only the density at a radial position of 0.4 mm is shown here, halfway between the center and the edge of the plasma jet effluent. The changes at this radial position can be used as a measure for the other radial positions in the effluent, as observed in Figure 4A and B.

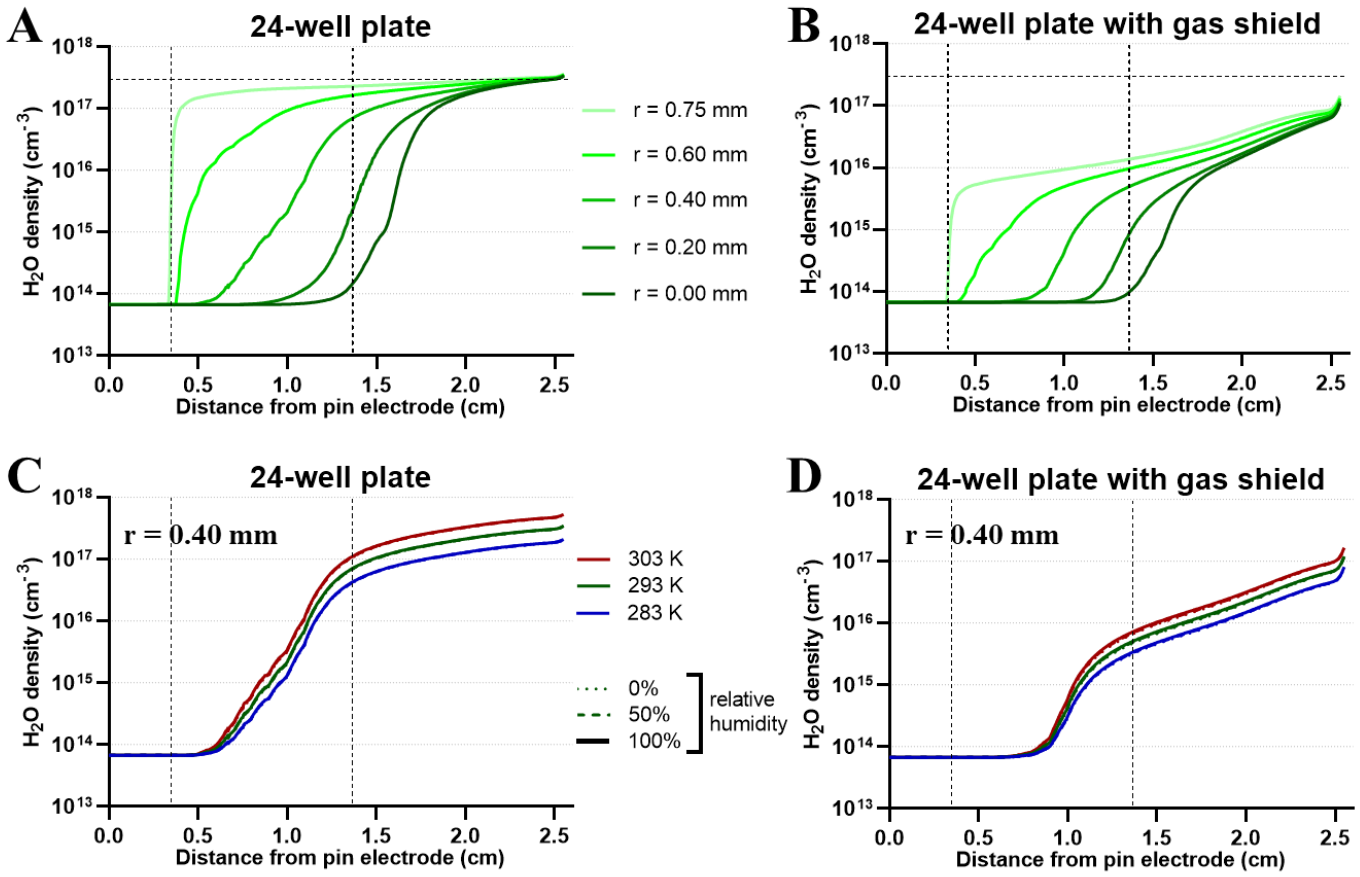

Figure 4 Calculated H_2O number density in the jet effluent, for different radial positions (A and B) and different ambient conditions (C and D). Results are shown for the case without (A and C) and with (B and D) gas shield. The first (x = 0.35 cm) and second (x = 1.35 cm) vertical dotted lines indicate the jet nozzle and the end of the plasma plume, respectively. The horizontal dotted line, indicating the number density in the surrounding air (at 1 atm and 293 K), is only shown for A and B, as it changes for different conditions. The different relative humidities in C and D overlap.

Two main conclusions can be drawn from Figure 4. First, we can see that the gas shield reduces the H_2O concentration throughout the effluent. Indeed, since the gas shield is composed of dry air, it causes the H_2O concentration in the effluent to drop up to a factor 20 compared to the case without gas shield. Still, as observed from Figure 4D, it does not eliminate the variation in the H_2O concentration caused by different ambient conditions. In fact, the relative difference stays unchanged: both with and without the gas shield, there is a factor 3 difference between H_2O density in the effluent at an ambient temperature of 283 K and 303 K. A second observation is that the ambient temperature is by far the main cause of the different H_2O densities in the effluent, both with and without the gas shield. Indeed, while the temperature determines which H_2O concentration in the air corresponds to a certain relative humidity, our model predicts almost the same rise in H_2O density for 0% and 100% relative humidity at each temperature. Therefore, the atmospheric water vapor cannot be the cause of the variation.

An additional source of H_2O in this treatment setup is the water that evaporates from the treated liquid surface. As gas from the jet flows over this surface, it takes with it the vapor that is present just above the surface and mixes it into the vortex present in the well. The vapor pressure of water is determined by the temperature, implemented into our model via Antoine's law. To confirm that it is the evaporated water that gives rise to the H_2O present in the jet effluent as opposed to the ambient water, we adapted our model so that it treats the H_2O originating from different sources (i.e., from impurities in the feed gas, from the ambient atmosphere and from evaporation at the liquid surface) as different species. The results are presented in Figure 5. Indeed, most of the water vapor in the jet effluent is evaporated H_2O from the treated liquid. Even without the gas shield, the ambient H_2O is kept relatively far away from the effluent, due to the backflow created by the well. In a way, this backflow induced by treatment of a well already acts as its own gas shield. Implementation of the actual shielding gas device then enhances the shielding effect, keeping ambient species even further away from the effluent (cf. Figure 5A). Additionally, the gas shield changes the flow field so that most evaporated water is guided outside of the well, decreasing the concentration of water vapor in the jet effluent (cf. Figure 5B).

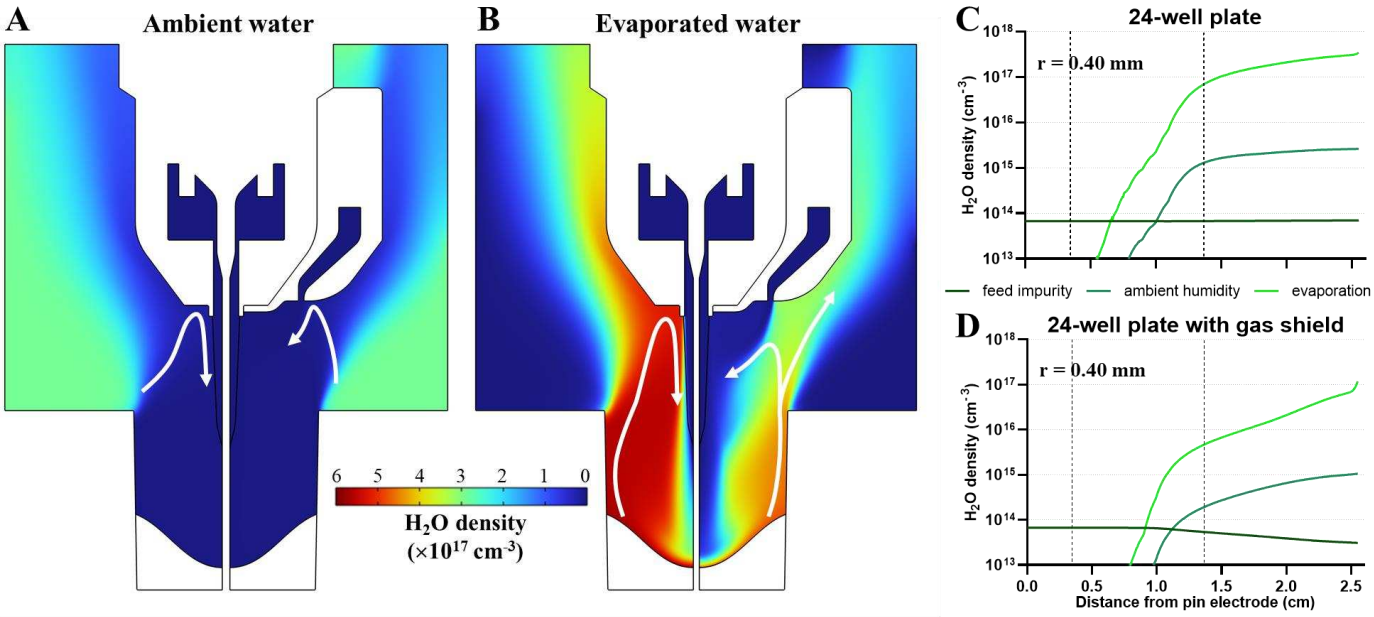

Figure 5 Calculated H_2O number density in the jet effluent originating from different sources. 2D profiles show the H_2O originating from the ambient humidity (A) or evaporation (B), both without and with gas shield. White arrows represent the main paths through which water mixes with the jet effluent. 1D profiles show the number densities originating from the different sources, i.e., ambient humidity, evaporation, and feed impurity, at a radial distance of 0.4 mm, without (C) and with (D) gas shield.

Apart from using a gas shield, another approach that can be used to reduce the effect of (different amounts of) water vapor in the ambient is by admixing H_2O into the feed gas of the plasma jet, in much larger amounts than the impurity levels typically already present. It was shown in literature that this admixed water vapor has a much larger influence than different humidities surrounding the effluent (57), effectively making a

variation in ambient humidity less relevant. When humidifying the feed gas (or shielding gas), the humidity should however still be actively controlled with e.g. a hygrometer (57), in order to obtain precise, reproducible treatments. Usually, H_2O admixtures are introduced into the feed gas of a plasma jet by leading (part of) the dry feed though a water bubbler. Since the vapor pressure of the water, and thus the amount of gaseous H_2O, depends on the temperature, different ambient temperatures can still influence the amounts of H_2O in the plasma, unless the bubbler is temperature controlled. In addition, depending on the liquid volume, continuous evaporation from the bubbler will cause the liquid water to cool down, changing the amount of H_2O in the gas over time. In practice, the kINPen is mostly used without admixed H_2O, and feed gas impurity forms only a small contribution. In these cases, most of the H_2O entering the active plasma zone originates from the ambient, and even more from evaporated water when treating a liquid-filled well (cf. Figure 5; note the logarithmic scale). Thus, it should be kept in mind that different ambient conditions, and especially the temperature, can cause variations in the treatment (16).

3.2 Effect of the treated well size

In the previous section we demonstrated that the backflow created by the treated well plays a role in determining the conditions in the plasma jet effluent, as it can induce a "self-shielding" effect. In literature, different well sizes are used for treatment of liquid and/or cells with a plasma jet. For the generation of plasma-treated liquids, even larger containers like beakers or petri dishes are often treated. To investigate the effect of the substrate geometry, we simulated the plasma jet over a 12-, 24-, 48-, and 96-well plate.

3.2.1 Well size effect without gas shield

In this section, we investigate how the geometry of the treated well influences the conditions experienced by the plasma jet, and thus the treatment itself. Figure 6A shows the N_2 density as calculated for the treatment of the four different well sizes, without a shielding gas. To indicate how the well geometry influences the flow field, we also show the main streamlines originating from the jet.

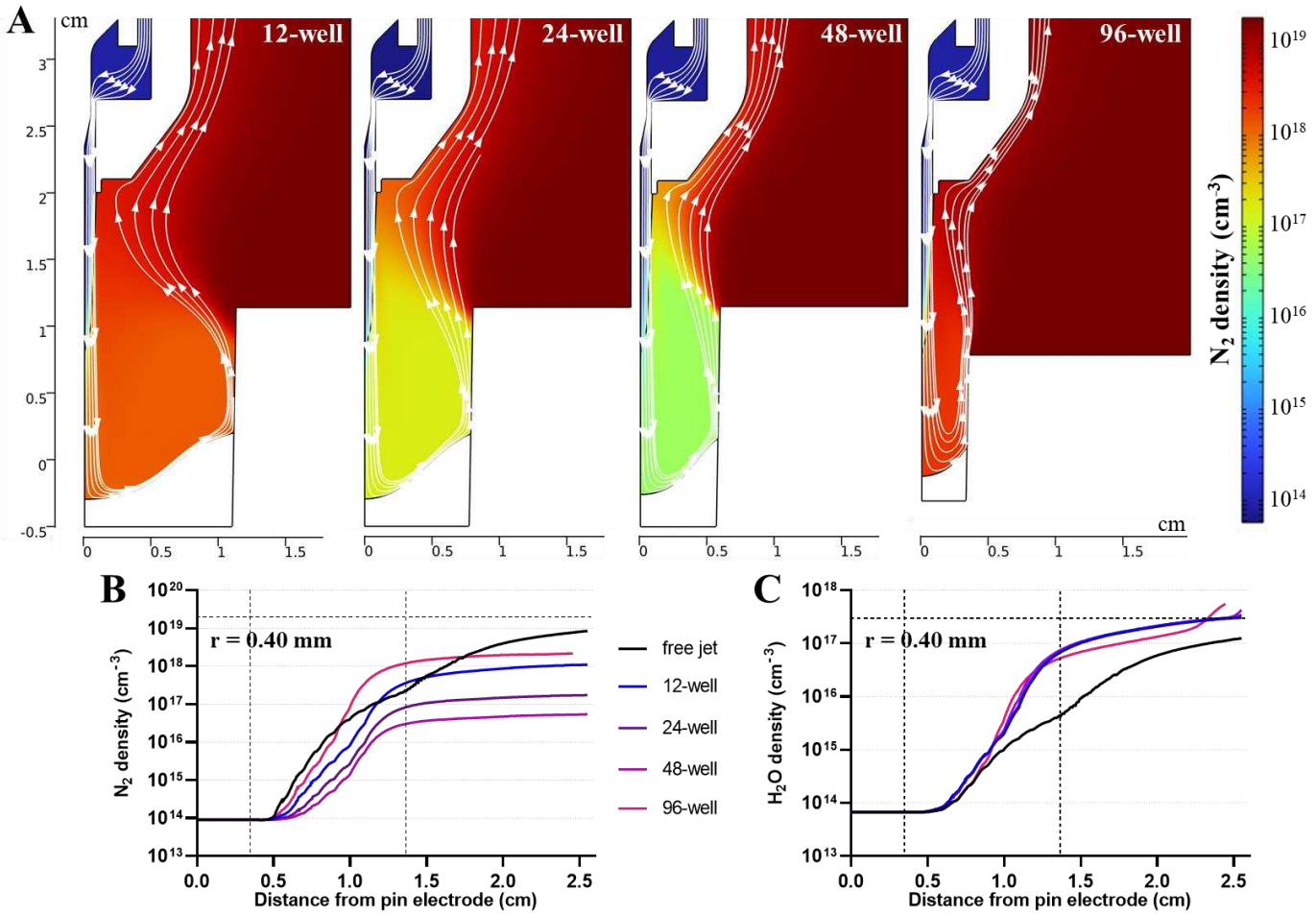

Figure 6 Influence of the well type on the flow field and N_2 density in 2D (A), and on the N_2 (B) and H_2O (C) density profiles in the jet effluent in 1D, without a shielding gas at 293 K. The flow lines in (A) originating from the jet are plotted in white. In B and C, comparison is also made with the result for a free jet. The H_2O density curves for the 12-, 24- and 48-well plates overlap, since the plasma effluent mainly mixes with evaporated water from the well.

Figure 6B and C depict the density of N_2 and H_2O in the jet effluent between the pin electrode and the liquid surface, for the different well types, as well as for a free jet. The difference in behavior with the free jet (i.e., without well plate) will be discussed below. Like in Figure 5, densities are shown for a radial position of 0.4 mm, but the behavior can be extended to the entire width of the effluent (cf. Figure 3). Clearly, the chosen well type significantly affects the N_2 density in the gas phase. As the well diameter decreases, the vortex in the well becomes more confined. This causes an increase in the velocity by which the backflow exits the well, and directs the backflow less towards the jet, effectively improving the "self-shielding" effect of the well-induced backflow. As a result, less ambient species, like N_2, enter the well and mix with the effluent. This trend is clearly visible up to the 48-well plate. For the 96-well plate, however, the N_2 density in the well and the effluent is the highest of all simulated wells (see Figure 6). The reason for this is twofold. First, because the well is so small, the gas flow is more turbulent than for the other wells, causing more turbulent

mixing in the region between the well interior and the surrounding gas. For example, the gas flow exiting the 48-well plate has a maximum turbulent dynamic viscosity of 1.8×10^{-4} Pa·s, while for the 96-well plate this is 7.1×10^{-4} Pa·s, causing a factor 9 and a factor 32 increase, respectively, in the diffusivity of N_2 over the normal molecular diffusion constant (cf. section 2.1.2). Secondly, whereas the other well types have the same depth (16.5 mm), the 96-well plate is more shallow (10.9 mm). Mohades *et al.* (60) have previously shown that the so-called rim-height of a well influences the amount of ambient gas that enters it, when treated with a plasma jet. As this rim height is lower for the 96-well plate than for the other investigated well plates, more N_2 is able to reach the interior of the well. It should be noted that, since the rim height depends on the amount of liquid in the well, the results from Figure 6B will be quantitatively different for smaller or larger liquid volumes. Indeed, more liquid will result in a lower rim height, causing more ambient gas to enter the well. We investigated the volumes typically used in experiments, as e.g. outlined in the standardized protocol by Tornin *et al.* (55).

While the N_2 in the effluent originates from the surrounding atmosphere, the H_2O in the effluent is mainly evaporated water from the treated liquid, as explained in the previous section. As the simulations were performed for the same temperature and thus the same vapor pressure, the H_2O densities in the effluent are similar regardless of the well type. Hence, the curves overlap, with only a small difference for the 96-well plate.

3.2.2 Experimental validation

To assess whether the change in effluent conditions caused by the well geometry in fact leads to a different treatment result for the treated liquid, we measured the concentration of long-lived RONS, i.e., H_2O_2, HNO_2 and HNO_3, in PBS after 60 seconds of treatment with the kINPen. Figure 7A shows the measured number of moles of each measured species in the different wells. As can be seen, the smaller wells take up less RONS. Yan *et al.* (61) also showed that the choice of well type, when treating a liquid with the kINPen, can change its reactive species uptake, and we see the same trend as the one they reported (61). However, while Yan *et al.* (61) attributed the lower species uptake by the smaller wells to the decreasing surface area through which the liquid can exchange species with the gas, Figure 7B clearly demonstrates that this cannot be the only explanation. If the surface area was the only cause, the RONS uptake per unit of surface area should be the same for each well type. Instead, more RONS seem to be taken up by the liquid in the smallest well per unit of surface area than by the largest well, and the surface area of the liquid and its reactive species uptake do not vary in the same way for the different well plates. Indeed, whereas the 12-well plate contains twice as much H_2O_2 as the 48-well plate, its liquid surface area is four times as large. Since the uptake of species by a liquid is determined by the concentration of that species above the liquid surface, this indicates that the concentrations of the species in the gas phase above the liquid are different, even though the sole difference is the type of well that is treated.

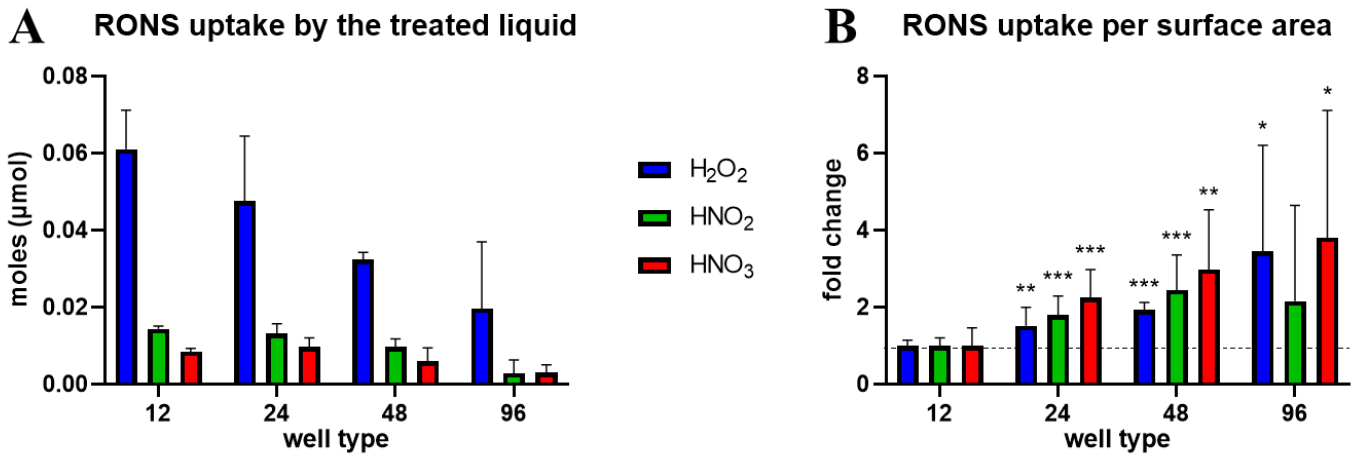

Figure 7 Experimentally measured RONS in the treated liquid for different well types, in absolute number of moles (A), and per unit of liquid surface area (B). Data is shown as the mean value and standard deviation of the replicates. For easy comparison between the different well types, the RONS uptake per surface area is plotted as fold change with respect to the 12-well plate, and the statistical significance of this difference is indicated (* = $p < 0.05$, ** = $p < 0.01$, *** = $p < 0.001$). Note that due to their different size, the wells contained different volumes of liquid (cf. section 2.2), meaning that the number of moles and the concentration do not follow the same trend. For instance, while the number of moles H_2O_2 as measured in a 12- and 48-well plate is 0.06 µmol and 0.032 µmol, respectively, their H_2O_2 concentrations after treatment are 30 µM and 65 µM.

The main chemical reaction leading to the formation of H_2O_2 in the gas phase by the kINPen is (32, 58):

$$OH + OH + M \rightarrow H_2O_2 + M \quad (R1)$$

$$k = 8.0\times10^{-31}\left(\frac{T}{300\ K}\right)^{-0.8}$$

Where M stands for a neutral collision partner, such as Ar. OH radicals are formed in the active plasma by the dissociation of water. It has been reported in literature that OH radical densities produced by a plasma jet correlate linearly with the H_2O density within a range relevant for the current study (58, 62). From the results shown in Figure 7B, we can deduce that a smaller size of the treated well leads to a higher gas phase concentration of H_2O_2 above the liquid. However, since the H_2O density in the jet effluent is the same regardless of the well type, according to our model (cf. Figure 6), the rise in H_2O_2 production cannot be due to reaction (R1). Contrary to H_2O, the calculated N_2 and O_2 densities in the effluent change significantly depending on the chosen well type (cf. Figure 6). Increasing levels of air entering the plasma will lead to increased production of primary and secondary RONS such as N and NO (56). Both species in turn react with OH via the following reactions (30, 32):

$$N + OH \rightarrow NO + H \quad (R2)$$

$$k = 4.7\times10^{-11}$$

$$NO + OH + M \rightarrow HNO_2 + M \quad (R3)$$

$$k = 7.4\times10^{-31}\left(\frac{T}{300\ K}\right)^{-2.4}$$

These reactions will compete with reaction (R1) and thus reduce the amount of H_2O_2 formed via OH radical recombination. This can explain the increasing H_2O_2 trend seen for the 12-, 24- and 48-well plate seen in Figure 7B. Indeed, decreasing $N_2(/O_2)$ densities in the smaller well sizes can lead to a higher rate of (R1), due to less competition with (R2) and (R3). On the other hand, the 96-well does not follow this trend. This is unexpected, since our model predicts the $N_2(/O_2)$ density in the effluent to be the highest when treating a 96-well plate (cf. Figure 6), while experimentally the highest average H_2O_2 concentration was found in the liquid. It is possible that our model does not yet accurately describe all mechanisms at play. Especially for the 96-well plate, which is a very small system, certain assumptions in the model may play a larger role, such as the stationary liquid surface that may affect the flow field in the gas. Still, the trends seen for the other well types do agree well between our model and experiments. Additionally, chemical reactions in the liquid may influence the results. Indeed, plasma-treatment of PBS can cause formation of ClO^- through reaction of Cl^- with atomic oxygen (63). H_2O_2 (and HNO_2) can, in turn, react with ClO^-, via e.g. the following reactions:

$$H_2O_2 + ClO^- \rightarrow Cl^- + H_2O + O_2 \text{ (R4)}$$

$$NO_2^- + ClO^- \rightarrow Cl^- + NO_3^- \text{ (R5)}$$

However, the kINPen, using Ar as the feed gas, leads to much smaller amounts of ClO^- in PBS compared to other CAP devices, e.g., the COST-jet operating with He/O_2 as feed gas (64). In addition, Van Boxem *et al.* (32) showed the stability of H_2O_2 in PBS for 2 hours after treatment with the kINPen. Still, the possibility of a small production of ClO^- cannot be excluded. The surface-to-volume ratio of the liquid in the investigated wells (i.e. the surface through which RONS can enter the liquid, compared to the volume in which they can react) is nearly the same for all wells, except for the 96-well plate. Thus, this may be an additional reason why its results in Figure 7 do not follow the qualitative trend explained above. Finally, it must also be noted that the experimental results for the 96-well plate in Figure 7 simply have a very large uncertainty. For example, the difference in HNO_2 uptake per surface area of the 96-well plate, compared to that of the 12-well plate, is not statistically significant. This large uncertainty can be explained in two ways. First, we showed in Figure 6 that, due to the higher turbulence and lower rim-height, more ambient gas mixes with the plasma effluent for the 96-well plate compared to the other well plates. This means that treatment of a 96-well plate will be inherently more susceptible to different relative humidities compared to the other well types. Second, the diameter of a 96-well is only 4.3 times larger than that of the kINPen nozzle. Small deviations from a perfectly centered position above the well may thus significantly influence the flow field in the well. As our model describes an ideal geometry, this may additionally form an explanation for why our model and our experiments do not follow the same trend for the 96-well plate only.

The trends plotted in Figure 7 for HNO_2 and HNO_3 are less straightforward to explain. Like for H_2O_2, the liquid takes up a higher amount per unit of surface area for decreasing well size, indicating higher gas phase concentrations. However, because the formation of HNO_2 and HNO_3 requires the presence of both N_2 and

O_2, and the concentrations of these species in the effluent decrease with smaller well sizes, as shown in Figure 6B, one would expect HNO_2 and HNO_3 to follow this trend. Instead, however, we see the opposite. HNO_2 is mainly formed via reaction (R3), while HNO_3 is formed through (30):

$$NO_2 + OH + M \rightarrow HNO_3 + M \quad \text{(R6)}$$

$$k = 4.6\times10^{-29}\left(\frac{T}{300\ K}\right)^{-0.8}\exp\left(-\frac{1180}{T}\right)$$

where NO_2 in turn is formed from NO. It was noted by Van Gaens *et al.* (33) that NO_2 production by the kINPen rises with increasing amounts of N_2 or O_2 only up to a certain point: above 0.1% O_2 content and 0.15% N_2 content, the NO_2 production decreases again. Mohades *et al.* (60) calculated lower concentrations of NO and NO_2 near the liquid in geometries where more N_2/O_2 from the ambient diffused into the well. Though both these observations are in line with the behavior we see here, they cannot be directly compared. In (33), N_2 and O_2 were supplied to the jet as admixtures in the feed gas, while in (60) a different type of plasma jet was simulated. A more in-depth analysis is thus necessary to fully explain the observed trends, which will be part of future work. Nevertheless, both our experimental and computational results show that the choice of treated well type can have a significant influence on the effluent conditions and, by extension, the treatment itself. This is important to keep in mind for plasma medicine applications.

3.2.3 Well size effect with gas shield

We also investigated how the chosen well geometry impacts the effluent conditions when a gas shield is employed. The results are depicted in Figure 8 in a similar way as Figure 6, for the different well types, as well as for a free jet. The difference in behavior with the free jet will also be discussed below. When implementing a gas shield, it is clear that the flow field changes drastically for different treated wells. An extreme case is the treatment of a 48-well plate. Because the edge of the well in this case is positioned at a similar radial position as the nozzle of the shielding gas device, the shielding gas does not blow into the well being treated, but instead into the wells surrounding it. The neighboring well for the 48-well plate is shown in Figure 8A to illustrate this. It should be noted that this second well is in fact treated in the model as a ring-shaped cavity surrounding the treated well, because the model is axisymmetric. However, this still illustrates the effect on the neighboring wells. For the other well types, Figure 8A shows the results of simulations without the neighboring well present. In these cases, we also performed simulations that included the neighboring well, but its inclusion had no effect on the results, and the flow did not enter the neighboring well like for the 48-well plate.

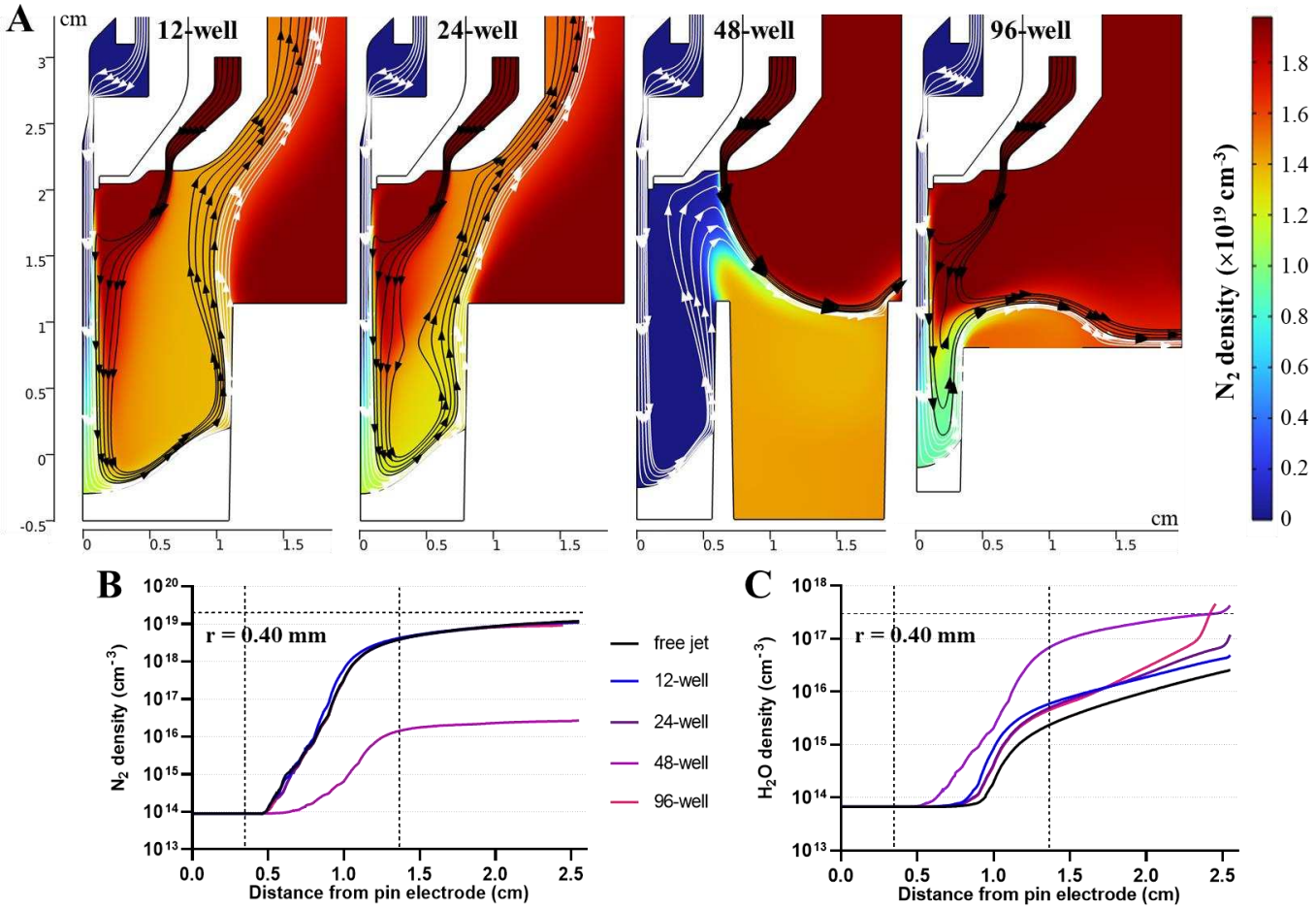

Figure 8 Influence of the well type on the flow field and N_2 density in 2D (A), and on the N_2 (B) and H_2O (C) density profiles in 1D, in the jet effluent, with a shielding gas at 293 K. The flow lines in (A) originating from the jet and the gas shield are plotted in white and black, respectively. In B and C, comparison is also made with the result for a free jet with gas shield. For the 48-well plate, a neighboring well is shown in (A), for clarity. For the other well types, the inclusion of a neighboring well has no effect on the flow field. The N_2 density curves for the 12-, 24- and 96-well plates overlap, since the plasma effluent mainly mixes with air supplied by the shielding gas.

We can thus expect that for the 48-well plate the gas shield will not actually provide a shielding effect, as is clear from the flow field in Figure 8A. Indeed, when comparing Figure 8 with Figure 6 we can see that there is little difference between, respectively, the N_2 and the H_2O density for the 48-well with or without a gas shield. For the other wells, the shielding gas does envelop the plasma jet effluent. Because in these cases, almost all N_2 that mixes with the effluent is supplied by the shielding gas, the N_2 density in the effluent is the same for the 12-, 24- and 96-well plate. The H_2O density is also very similar for these three well types. As discussed in section 3.1, the H_2O that mixes with the effluent is mainly evaporated water from the treated surface. The H_2O density is lower with shielding, because the flow field caused by the shielding gas for the three wells is such that it guides the evaporated water away from the jet nozzle, instead of towards it like in

the cases without shielding. Overall, our results indicate that the gas shield is able to induce a controlled environment surrounding and mixing with the jet effluent, regardless of the treated well type, although in some cases, like for the 48-well plate in this setup, the substrate geometry can influence the flow field in such a way that the shielding gas does not at all behave as intended.

3.2.4 Unintended effects on neighboring wells

The fact that the shielding gas blows into the wells surrounding the treated well, for the 48-well plate shown in Figure 8, does not only cause the gas shield to not operate as intended. Along with the shielding gas, much of the effluent from the plasma jet passes through the neighboring well. This means that in this geometry, wells could be unintendedly affected by the treatment of other wells close by.

The RONS produced by a plasma jet can be divided into three groups (43). These are (i) short-lived species, which quickly react away after the end of the active plasma zone (some even before reaching the liquid), (ii) long-lived species with a high Henry's constant, and (iii) long-lived species with a low Henry's constant. For a flow field such as that of the 48-well plate in Figure 8, short-lived species are unlikely to reach the neighboring wells, because they react away quickly. Long-lived species with a high Henry's constant can survive long enough, but are also unlikely to reach the neighboring wells because they will mostly be taken up by the liquid in the treated well, more so for higher Henry's constants. However, long-lived species with a low Henry's constant, that are thus only taken up by the treated liquid in small amounts, are able to reach the surrounding wells and dissolve in the liquid therein. To illustrate this, we performed simulations where a 10^{15} cm^{-3} O_3 was supplied at the inlet of the plasma jet, similar to produced amounts of O_3 reported in literature (56), while the neighboring well (also shown in Figure 8A) was filled with liquid. Figure 9A shows the O_3 density in the gas and liquid phase, for a 48-well plate. Indeed, the flow field in this case guides a substantial amount of O_3 to the liquid surface in the neighboring well, where it subsequently dissolves.

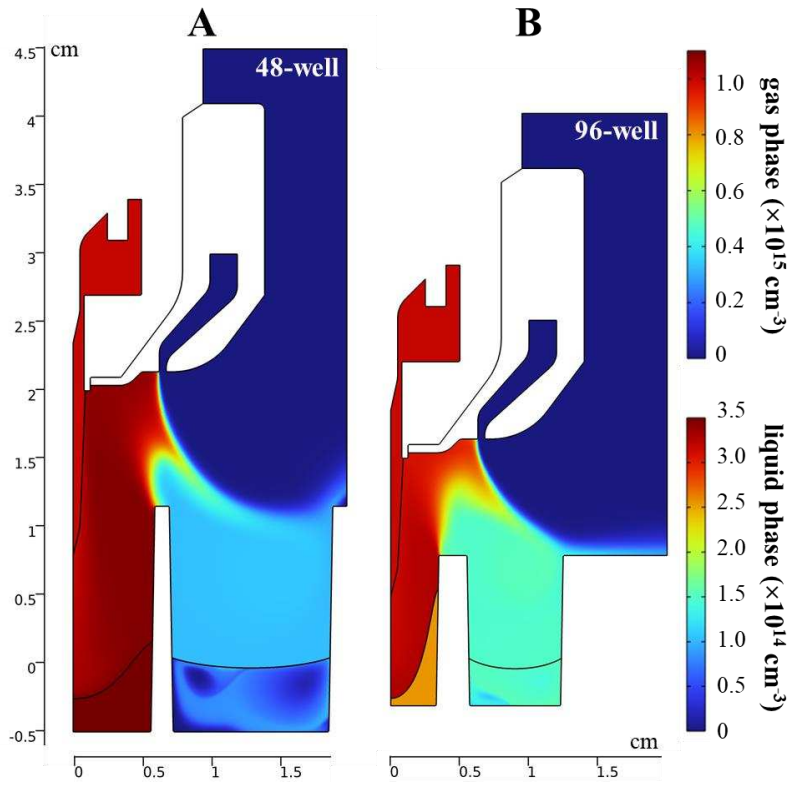

Figure 9 Ozone density in the gas and liquid phase of both the treated and neighboring well when the setup geometry causes the shielding gas to blow into the wells surrounding the treated well. (A) 48-well plate with a treatment gap of 2 cm. (B) 96-well plate with a treatment gap of 1.5 cm. An ozone density of 10^{15} cm^{-3} is supplied by the jet, based on reported produced densities in literature (56).

The effect occurs when the radius of the treated well is comparable to (or smaller than) the radius of the gas shield nozzle, in combination with a strong enough backflow from the well to push away the shielding gas. For instance, for a 96-well plate with 20 mm gap between the liquid and the plasma jet nozzle, as discussed in section 3.2.3, the flow does not affect the neighboring well, while for a smaller gap of 15 mm, and thus a stronger backflow, the same effect as for the 48-well plate with 20 mm gap can be seen (cf. Figure 9B).

3.2.5 Comparison with the free jet

As is clear from the previous sections, the choice of treated substrate will influence the treatment of the substrate itself. To emphasize this influence, Figure 6B and Figure 8B also show the density profiles of N_2 and H_2O as calculated for the free jet, i.e., without treated substrate. Due to the lack of a backflow from the treated well, the N_2 density without a shielding gas is significantly different for the free jet (cf. black curve in Figure 6B), which confirms again that caution should be taken when comparing results (like produced RONS densities) for the free jet with those gathered when treating a well. With a shielding gas, the N_2 density is independent of the well geometry (except for the 48-well), and the same as for the free jet, since in these

cases most N_2 mixing with the effluent is supplied by the shielding gas, confirming again that the shield is able to create a controlled environment. However, it should be kept in mind that the effect is not the same as a controlled atmosphere around the jet.

The H_2O density without shielding is lower for the free jet than for the treatment of any well type, which is to be expected, since without a treated liquid surface no evaporated water is present, and all H_2O in the effluent stems from the ambient humidity. The density is however higher than the H_2O density coming from the ambient shown in Figure 5B, because the “self-shielding” effect caused by the induced backflow from the well is absent here. This also means that the free jet is far more susceptible to varying ambient humidity, which is shown in Figure 10A. With the gas shield, one would expect that the lack of an evaporating liquid surface beneath the jet, and the presence of a shielding flow separating the effluent from the ambient, would cause the H_2O density to barely rise above the impurity level in the feed gas. Surprisingly, as shown in Figure 10, the H_2O density is similar with and without a gas shield. The position from which concentrations start to rise is increased slightly, but by the end of the plasma plume (x = 1.35 cm) the densities are at the same level as without shielding gas. This indicates that the gas shield does not efficiently shield the jet effluent from the surrounding atmosphere at all. In the following section, the reason for this will be elucidated.

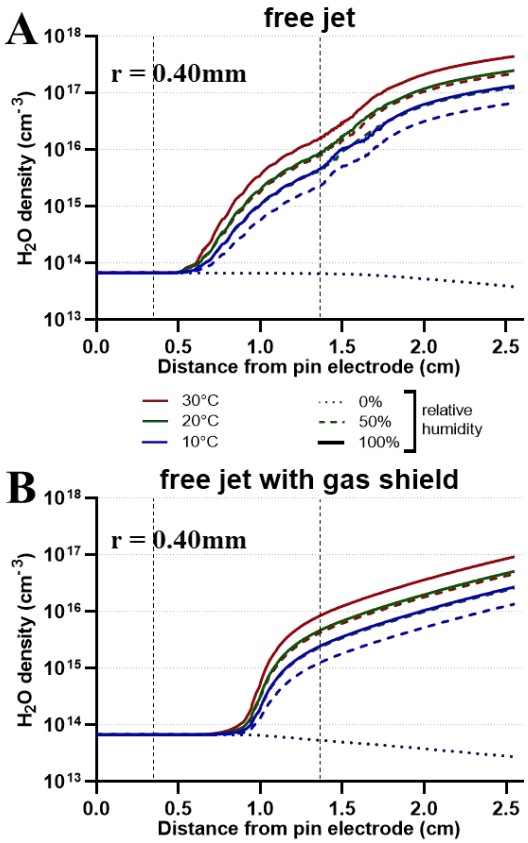

Figure 10 H_2O density in the jet effluent as calculated for the free jet, without (A) and with (B) gas shield, for three different ambient temperatures and three different relative humidities. As all water mixing with the jet originates from the ambient humidity, there is no rise in H_2O density for 0% relative humidity (see dotted line), and the curves for the three temperatures overlap.

3.3 Effect of gas shield geometry

In literature, the effectiveness of using a gas shield was shown by Reuter *et al.* (17), both experimentally and with a simple CFD model. The most notable difference between their investigation and our study is that a different shielding gas device was used, with a different geometry. While in (17) the device was made in-house, we opted (with the interest of reproducibility and a clinical setting in mind) for a device specifically made for the kINPen by Neoplas (65). Importantly, when we adapt our model to the geometry shown in (17), our computational results show efficient shielding for the free jet: any influence from the ambient atmosphere is pushed back by the gas shield until after the plasma plume has ended as illustrated in Figure 11B. Moreover, the different shield geometry also significantly changes the conditions in the plasma effluent above a well plate, as shown in Figure 11C: the rise in H_2O only happens after the end of the plasma plume (i.e. providing better shielding), and the amount of N_2 that mixes with the effluent is reduced.

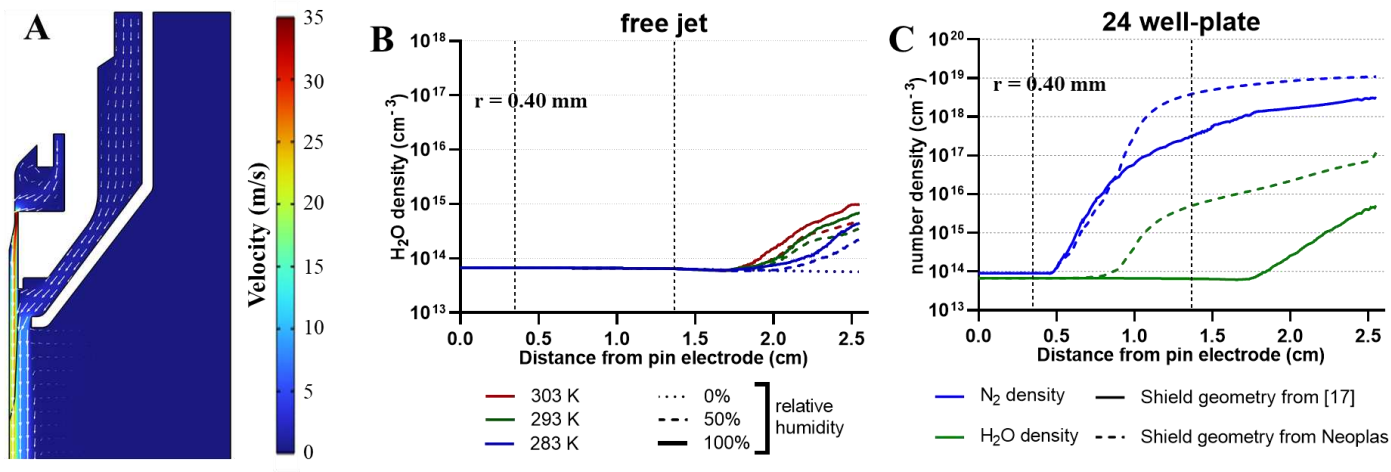

Figure 11 Calculated flow field (A) and H_2O number density in the jet effluent, for a free jet (B), for the shielding gas geometry used in (17). Number density of N_2 and H_2O in the effluent above a 24-well plate is also shown for both the shield from (17) and the shield from Neoplas (used throughout the paper), for 293 K and 50% relative humidity (C). It is important to note that the shape of the liquid water surface was kept unchanged for the different shield geometry. This will not be entirely correct: the different geometry changes the flow field, and e.g. slows stagnation of the effluent velocity, which will in turn induce a different liquid surface shape. However, we believe this effect is of minor importance for the message of this figure.

3.3.1 Experimentally testing shielding efficiency

To confirm that the shielding gas device used in our model so far does not provide efficient shielding, we experimentally tested different shielding gas compositions for treatment of a liquid sample, followed by measurement of long-lived RONS in the treated liquid. It has been shown in literature that when the plasma jet effluent is efficiently shielded from the environment, different shielding gas compositions can significantly change the RONS-composition of a treated liquid. For example, by using a shielding gas devoid of N_2, the production of nitrogen-containing species can effectively be prevented (19, 66). However, the results in Figure 12A show that HNO_2 and HNO_3 are still produced in large amounts when an Ar/O_2 shielding gas is used. Moreover, the production of the measured RONS is similar regardless of the shielding gas composition. This shows that despite the shielding, species from the ambient, like N_2, still make it into the jet effluent in significant amounts with this gas shield. This is also reflected by the measured response of melanoma cell line A375 to the plasma treatment, shown in Figure 12B: there is little difference between the results for the different shielding gas compositions. The difference with the treatment without shielding gas mirrors the measured H_2O_2 uptake, shown in Figure 12A. Note that the RONS measurements and the cell experiments were performed in different liquids. For the species measurements, PBS was used to prevent consumption of the long-lived RONS before measurement. For the cell experiments, the cells were treated in cell medium, which contains organic biomolecules that can act as scavengers for plasma-produced RONS. The response seen in Figure 12B is thus not only the result of the primary species produced by the plasma, but also of secondary species such as oxidized biomolecules, which also affect the cancer cells (67).

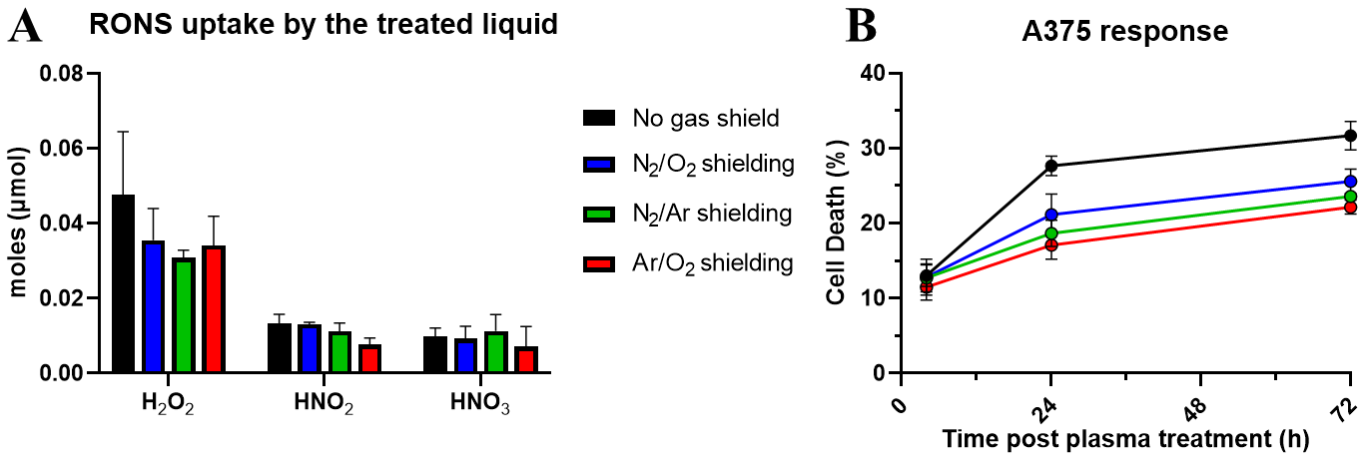

Figure 12 (A) Experimentally measured RONS uptake in treated liquid after 60 seconds of treatment time, for different shielding gas compositions. (B) Response of A375 cancer cells to the treatment, using the same treatment conditions as in (A). Data is shown as the mean value and standard deviation of the replicates. Cell death was measured 4, 24 and 72 h after the treatment.

3.3.2 Underlying reason for the different shielding efficiencies

The question remains what the reason is for the large difference in shielding efficacy seen when comparing Figure 11 with Figure 4B. One of the most notable differences between the two shield geometries is that the radial distance between the shielding nozzle and the jet nozzle is larger for the shield geometry used in the present study. At first glance, one would expect that increasing the radial position of the shielding nozzle could be beneficial, as it keeps the ambient further away from the plasma jet. However, as was visible in Figure 2, a vortex forms in the region between both nozzles. This vortex effectively "pulls in" species towards the jet effluent. In fact, this vortex acts in a similar way to the recirculation zone generated by bluff-body stabilization, used in combustion. In this field, the formation of a recirculation zone between the two nozzles is used to enhance fuel-air mixing and stabilize the flame (68, 69).

For the free jet, the species that are pulled in are those from the ambient atmosphere, explaining why in Figure 10 there is only a small difference between the case with and without gas shield. When the jet is positioned above a well plate, the species that are pulled in by the vortex are mainly those in the backflow coming from the well (explaining why the evaporated water so significantly affects the H_2O density in the jet effluent, while for the shield geometry in Figure 11 this is far less the case). However, species from the ambient also still make it into the effluent, as seen in Figure 5 and Figure 12. Finally, for a 96-well plate, we can see in Figure 8 that backflow coming from the well is directed outwards, unlike for the other well types where the induced backflow is directed upwards. This means that the gas next to the vortex between the jet nozzle and the shield nozzle is mainly the ambient atmosphere. Indeed, as shown in Figure 13, the ambient humidity plays a far larger role in this case than for the other well types, more akin to the situation without a treated well.

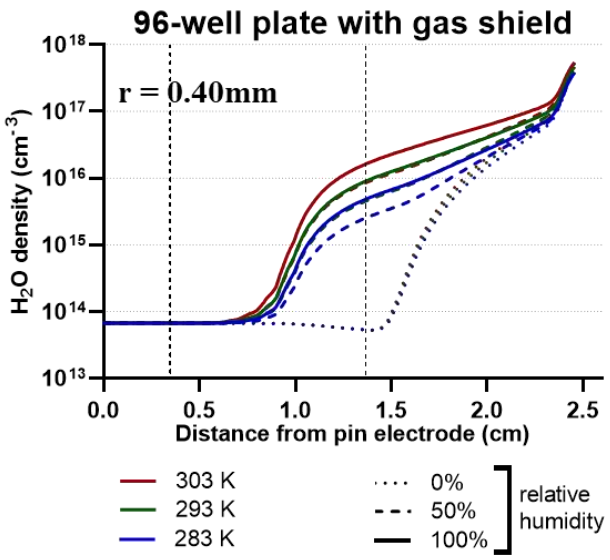

Figure 13 H_2O number density in the jet effluent as calculated for the 96-well plate with shielding gas.

3.3.3 Effect of the shield nozzle position and width

To investigate the effect of different gas shield geometries in more detail, we present here a systematic study of the effect of the gas shield geometry. Indeed, since its introduction by Reuter *et al.* (17), different gas shield geometries have been used in both modelling and experimental works (19, 35, 44). To the best of our knowledge, however, the influence of a change in shielding gas geometry on its efficacy has rarely been reported. In the following, we will use our model to investigate the effect of the gas shield geometry on the conditions in the plasma effluent, and its ability to shield the plasma effluent from the ambient. To investigate this in a general way, we simplified the model geometry, as shown in Figure 14A. Like in the previous sections, we will discuss the H_2O density and the N_2 density in the effluent (while O_2 acts in the same way as N_2).

Four main parameters can be adjusted in the shielding gas device geometry, i.e. (i) the axial and (ii) radial position of the shielding nozzle compared to the plasma jet nozzle, (iii) the width of the shielding nozzle, and (iv) the flow direction of the shielding gas relative to the plasma effluent. This section will present the effect of the first three parameters, while the flow direction will be discussed in section 3.3.4 below.

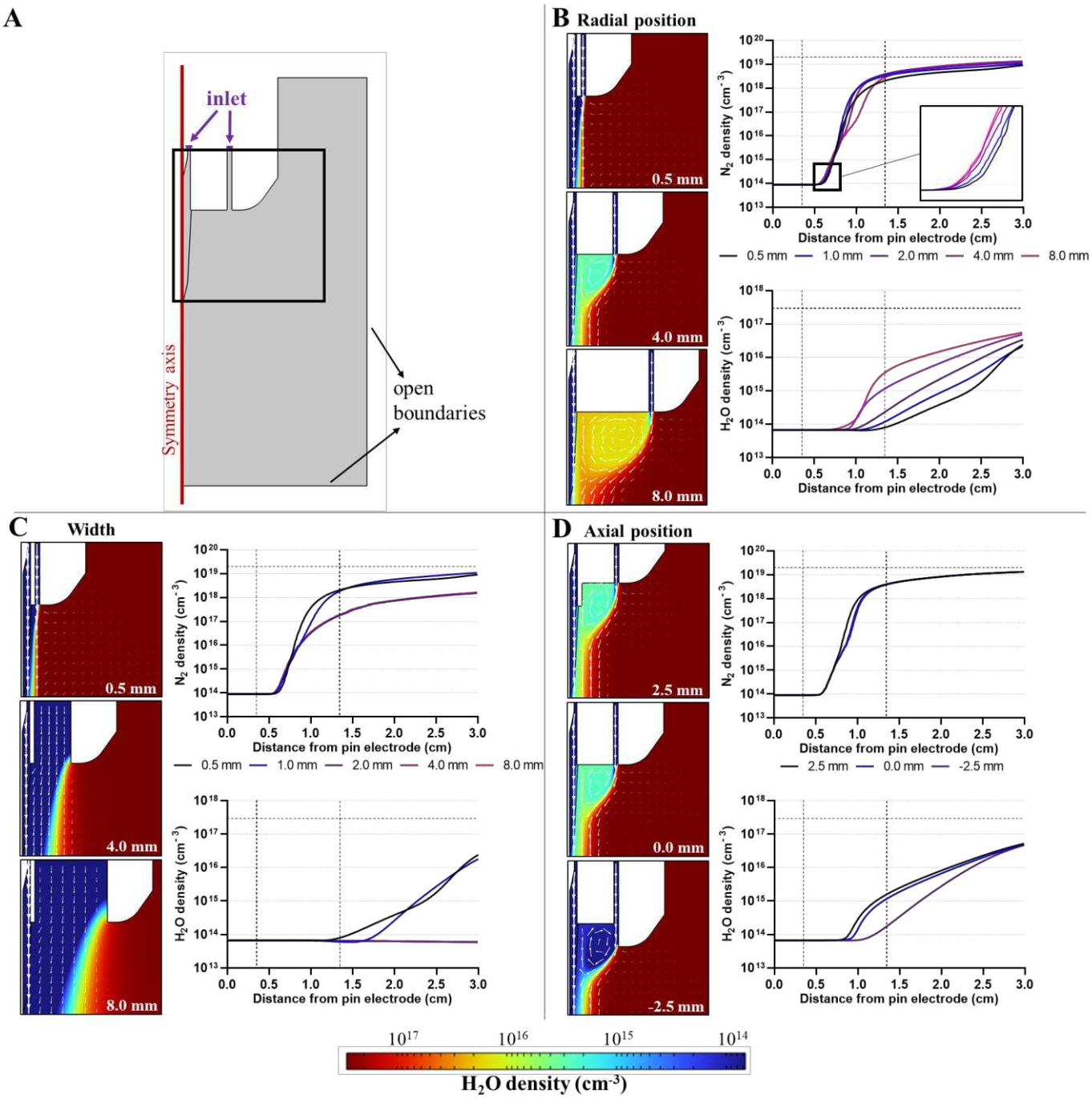

Figure 14 Effect of the gas shield geometry on the N_2 density and H_2O density in the plasma effluent. (A) shows the basic geometry of the jet nozzle and gas shield nozzle. The investigated parameters are (B) the radial position, (C) width and (D) axial position of the gas shield nozzle relative to the plasma jet nozzle. The 2D plots show the ambient H_2O density, with white arrows representing the flow field. In (A) the black box indicates which part of the geometry is shown in these 2D plots. The 1D plots depict the N_2 and H_2O number density in the plasma effluent, at a radial position of 0.40 mm, as a function of distance from the pin electrode for the different simulated gas shield geometries.

In (C), the curves for 2.0, 4.0 and 8.0 mm overlap. Note that the color scale is logarithmic to clearly visualize the differences.

Figure 14B illustrates the effect of the radial position of the shielding gas nozzle compared to the outer diameter of the plasma jet nozzle. A large radial distance between both nozzles causes formation of a vortex, like discussed previously in section 3.3.2, that accumulates species from the ambient atmosphere. As the radial distance decreases, this vortex becomes smaller, and the density of ambient species in it decreases. At very small radial distance between the nozzles, the vortex disappears completely. This trend is clearly visible for the H_2O density, on which the radial distance (and by extension, the size of the formed vortex) has a very large influence. For larger radial distances, the H_2O density in the plasma effluent rises much faster. Additionally, larger radial distances also decrease the axial position at which the rise in density starts. For the largest simulated radial distance (8 mm), the H_2O density in the plasma effluent (at a radial position of 0.4 mm) starts rising at 7 mm from the pin electrode. When the radial distance is small enough to prevent formation of the vortex, this rise in H_2O density only occurs near the very end of the plasma plume. This means that smaller radial distances between the jet and shielding nozzle, or in other words, a more confined shielding curtain around the plasma effluent, provides a better shielding effect. The same general trend is present for the N_2 density. A larger radial distance between the jet and shielding nozzle decreases the distance from the pin electrode at which the N_2 density in the plasma effluent starts to rise, and it increases the amount of N_2 in the effluent. Only at the end of the visible afterglow, around 10 mm from the pin electrode, the behavior is different, and no clear trend is visible.

Figure 14C shows the influence of the width of the shielding gas nozzle. It can be seen that increasing the gas curtain width causes a strong drop in the amount of H_2O that is able to mix with the plasma effluent, as the ambient is kept further away. This trend is opposite to that for an increasing radial distance between the plasma jet nozzle and the shielding gas nozzle. Indeed, increasing the radial position of the shield gas nozzle also keeps the ambient further away from the plasma jet, but this actually increases the amount of ambient H_2O that mixes with the jet effluent, due to the vortex creation. This further emphasizes the importance of the vortex that can form between the jet effluent and the shield effluent (note that in Figure 14B and Figure 14C the outer diameter of the gas shield is the same for each simulated condition, respectively). For the N_2 density, two behaviors can be seen. For small shield nozzle widths (0.5 -1 mm) the N_2 mixes with the plasma effluent in higher amounts compared to large nozzle widths (2 – 8 mm). This can be attributed to the fact that, for a large nozzle width, the flow is far less turbulent, causing much less turbulent mixing between the N_2 from the shielding gas and the plasma effluent. These two behaviors are in fact also visible for the H_2O density, indicating that turbulent mixing also plays a role in the mixing of the plasma effluent with the ambient atmosphere.

Finally, Figure 14D depicts the influence of the axial position of the shielding gas nozzle. The N_2 density in the plasma effluent is mostly unaffected by this change in geometry. For the H_2O density, increasing the axial position (i.e., if the shield nozzle position is higher than the jet nozzle position in the geometry of Figure 14A) has only a small effect. Lowering the axial position of the shield nozzle however significantly reduces

how quickly the ambient gas, as seen by the H_2O density, mixes with the plasma effluent. This is to be expected, because it simply takes longer before the ambient can start diffusing towards the jet effluent. Though the results in Figure 14D are only shown for the case where a vortex between the jet nozzle and shield nozzle forms, the trends are the same for the case where no vortex can form.

It should be kept in mind that these simulations were performed for the free jet. When treating a well plate, the backflow from the well can in some cases push back the shielding gas, which may cause unintended effects, as discussed in section 3.2.4. To emphasize this, Figure 15A shows the effect of the radial position of the shielding gas nozzle, like also depicted in Figure 14B, but for the treatment of a 24-well plate (with a 2 cm treatment gap). For a radial distance of 0.5 and 4.0 mm, the shielding gas flow is unaffected, although in these cases most of the H_2O that mixes with the plasma effluent (and accumulates in the vortex, when formed) is evaporated water as opposed to H_2O from the ambient air, as shown in Figure 15B. For a radial distance of 8.0 mm, however, the radial position of the shielding gas nozzle becomes similar to that of the well edge, and no vortex forms. Instead, the shielding gas blows into the wells surrounding the treated well. Additionally, although Figure 14C indicates that increasing the shielding nozzle width gives a better shieling effect, a wider shielding curtain makes it easier for the backflow from the well to push back the shielding gas.

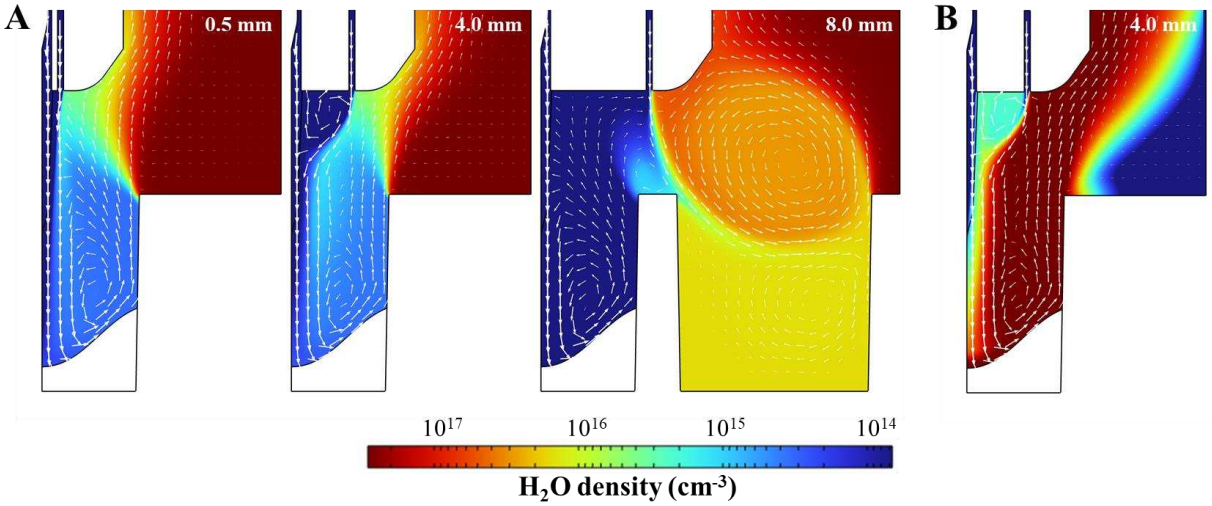

Figure 15 Effect of the well-induced backflow on a gas shield, for different radial distances of the shielding gas nozzle. (A) Ambient H_2O density in the system. For the case with a radial distance of 8.0 mm, the neighboring well is shown, for clarity. (B) Evaporated H_2O density in the system, for the gas shield with a radial distance of 4.0 mm. White arrows represent the flow field.

3.3.4 Effect of the flow direction

Apart from the position of the shielding gas nozzle relative to the plasma jet nozzle, and its width, the flow direction relative to the plasma effluent can be adapted. In literature, different gas shields are depicted that direct the shielding curtain parallel to the plasma effluent (35), or direct it towards the plasma effluent

diagonally (44, 70) or perpendicularly (17). Figure 16 shows the influence of the flow direction of the shielding gas, for a small radial distance between the jet nozzle and the shielding gas nozzle. It can be seen that both the diagonal and perpendicular flow direction induce less mixing of the jet effluent with H_2O from the ambient, compared to the parallel flow. The reason is that for these two cases there is much less turbulent mixing, similar to the effect of the shielding nozzle width discussed in the previous section, which causes the ambient air to penetrate into the jet effluent far slower. This behavior was also noted by Gazzah *et al*. (71), who reported reduced mixing in a jet with co-flow by directing the co-flow towards the jet effluent. This also explains the N_2 profiles plotted in Figure 16: less N_2 mixes with the jet effluent for the diagonal and perpendicular compared to the parallel flow direction. Note that here, the same two behaviors can be seen as in Figure 14C.

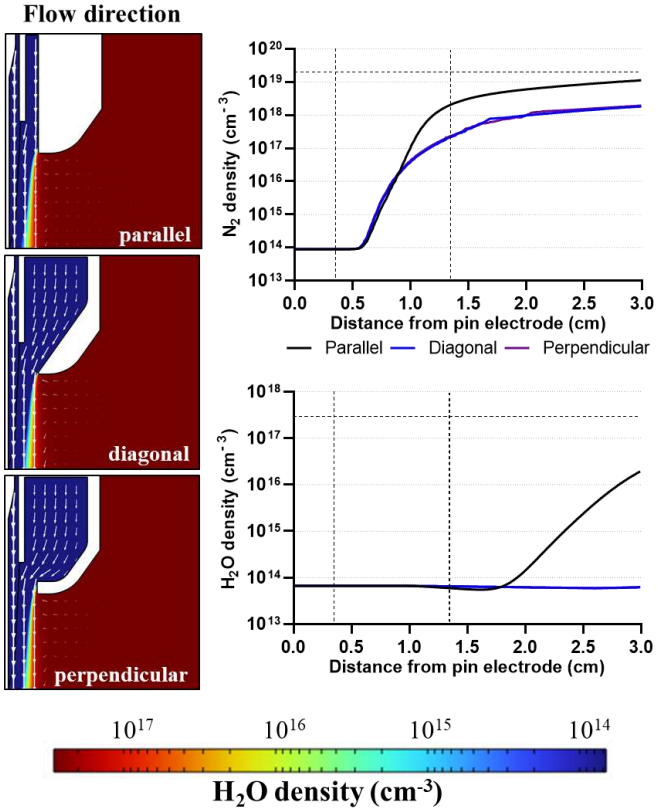

Figure 16 Effect of the flow direction of the gas shield, relative to the flow from the plasma jet, on the N_2 density and H_2O density in the plasma effluent. The 2D plots show the ambient H_2O density, with white arrows representing the flow field. The 1D plots show the N_2 and H_2O number density in the plasma effluent as a function of distance from the pin electrode for the different simulated flow direction of the gas shield.

4. CONCLUSION

We investigated how *in vitro* treatment with a plasma jet is affected by the geometry of the treatment setup, i.e., the chosen well type, and the use of a shielding gas device. For this purpose, we developed a computational 2D-axisymmetric model of the kINPen plasma jet above a liquid water surface, with and without gas shielding, to investigate the mixing of the plasma jet effluent with the ambient N_2, O_2 and H_2O. These molecules drive the formation of RONS by the plasma, and thus their mixing with the plasma influences the treatment effect. Simulations were performed for different ambient temperatures and relative humidities.

Both our computational and experimental results show that the choice of treated well type can significantly influence the effluent conditions and, by extension, the treatment itself. The backflow created by the treatment of a well plate plays a role in determining the conditions in the plasma jet effluent, as it can induce a "self-shielding" effect. Because this flow field depends on the size of the treated well, mixing of the plasma with the ambient will be different for different treated wells, causing changes in the RONS formation. Additionally, because the self-shielding keeps the surrounding atmosphere away from the plasma effluent, evaporation of water in the treated well forms the main contributor to the H_2O that enters the plasma plume. The use of a shielding gas provides a consistent supply of gas, and is able to induce a controlled environment surrounding and mixing with the jet effluent, regardless of the treated well type. However, in some cases, like for the 48-well plate in this setup, the substrate geometry can influence the flow field in such a way that the shielding gas does not at all behave as intended. When the radius of the treated well is comparable to (or smaller than) the radius of the gas shield nozzle, in combination with a strong enough backflow from the well, the shielding gas can be pushed away. In this case, the long-lived RONS with a low Henry's constant, such as O_3, may enter the wells surrounding the treated well, causing unintended effects of the treatment to these neighboring wells. Furthermore, it should be taken into account that the flow of a gas shield can enhance the amount of N_2 and O_2 that mixes with the plasma effluent. This means that caution must be taken when diagnostics in the presence of a gas shield are compared to experiments without a gas shield, as they do not entail the same (quantitative) conditions in the active plasma zone.

Finally, we systematically investigated the effect of different gas shield geometries, i.e., the radial and axial position of the shielding gas nozzle, its width, and the flow direction relative to the plasma jet flow. Overall, the largest effect was seen for the radial position of the shielding gas nozzle. When this increases, a recirculation zone can arise between the shielding curtain and the plasma effluent, which pulls in species from the ambient, severely changing the conditions in the plasma effluent. In this way, we showed that the gas shield design can have a substantial effect on the shielding efficiency.

Altogether, our results provide a deeper understanding of how the choice of setup geometry, such as the treated well and the use of a gas shield, can influence the conditions in the plasma effluent and, by extension, the plasma treatment itself.

DATA AVAILABILITY STATEMENT

Any data that support the findings of this study are included within the article.

ACKNOWLEDGEMENTS

We acknowledge financial support from the Fund for Scientific Research (FWO) Flanders (Grant ID 1100421N, G033020N and 1SD6522N). This article is based upon work from COST Action CA20114 PlasTHER "Therapeutical Applications of Cold Plasmas", supported by COST (European Cooperation in Science and Technology). We also thank I. Tsonev, S. Van Hove, R. De Meyer and R. Vertongen for their help with the model development, and valuable input.

REFERENCES

1. Braný D, Dvorská D, Halašová E, Škovierová H. Cold atmospheric plasma: A powerful tool for modern medicine. International journal of molecular sciences. 2020;21(8):2932.
2. Laroussi M. Plasma medicine: a brief introduction. Plasma. 2018;1(1):47-60.
3. Bekeschus S, von Woedtke T, Emmert S, Schmidt A. Medical gas plasma-stimulated wound healing: Evidence and mechanisms. Redox biology. 2021;46:102116.
4. Boeckmann L, Schäfer M, Bernhardt T, Semmler ML, Jung O, Ojak G, et al. Cold atmospheric pressure plasma in wound healing and cancer treatment. Applied Sciences. 2020;10(19):6898.
5. Keidar M. Plasma cancer therapy: Springer; 2020.
6. Gorbanev Y, Vervloessem E, Nikiforov A, Bogaerts A. Nitrogen fixation with water vapor by nonequilibrium plasma: toward sustainable ammonia production. ACS Sustainable Chemistry & Engineering. 2020;8(7):2996-3004.
7. Onyshchenko I, De Geyter N, Morent R. Improvement of the plasma treatment effect on PET with a newly designed atmospheric pressure plasma jet. Plasma Processes and Polymers. 2017;14(8):1600200.
8. Reuter S, von Woedtke T, Weltmann K-D. The kINPen—a review on physics and chemistry of the atmospheric pressure plasma jet and its applications. Journal of Physics D: Applied Physics. 2018;51(23):233001.
9. Bekeschus S, Freund E, Spadola C, Privat-Maldonado A, Hackbarth C, Bogaerts A, et al. Risk assessment of kINPen plasma treatment of four human pancreatic cancer cell lines with respect to metastasis. Cancers. 2019;11(9):1237.
10. Bekeschus S, Schmidt A, Weltmann K-D, von Woedtke T. The plasma jet kINPen–A powerful tool for wound healing. Clinical Plasma Medicine. 2016;4(1):19-28.
11. Graves DB. The emerging role of reactive oxygen and nitrogen species in redox biology and some implications for plasma applications to medicine and biology. Journal of Physics D: Applied Physics. 2012;45(26):263001.
12. Privat-Maldonado A, Schmidt A, Lin A, Weltmann K-D, Wende K, Bogaerts A, et al. ROS from physical plasmas: Redox chemistry for biomedical therapy. Oxidative medicine and cellular longevity. 2019;2019.
13. Lietz AM, Kushner MJ. Molecular admixtures and impurities in atmospheric pressure plasma jets. Journal of Applied Physics. 2018;124(15):153303.
14. Iséni S, Reuter S, Weltmann K-D. NO2 dynamics of an Ar/Air plasma jet investigated by in situ quantum cascade laser spectroscopy at atmospheric pressure. Journal of Physics D: Applied Physics. 2014;47(7):075203.

15. Reuter S, Tresp H, Wende K, Hammer MU, Winter J, Masur K, et al. From RONS to ROS: tailoring plasma jet treatment of skin cells. IEEE Transactions on Plasma Science. 2012;40(11):2986-93.
16. Winter J, Wende K, Masur K, Iseni S, Dünnbier M, Hammer M, et al. Feed gas humidity: a vital parameter affecting a cold atmospheric-pressure plasma jet and plasma-treated human skin cells. Journal of Physics D: Applied Physics. 2013;46(29):295401.
17. Reuter S, Winter J, Schmidt-Bleker A, Tresp H, Hammer MU, Weltmann K-D. Controlling the ambient air affected reactive species composition in the effluent of an argon plasma jet. IEEE Transactions on Plasma Science. 2012;40(11):2788-94.
18. Bekeschus S, Iseni S, Reuter S, Masur K, Weltmann K-D. Nitrogen shielding of an argon plasma jet and its effects on human immune cells. IEEE Transactions on Plasma Science. 2015;43(3):776-81.
19. Schmidt A, Bekeschus S, Jablonowski H, Barton A, Weltmann K-D, Wende K. Role of ambient gas composition on cold physical plasma-elicited cell signaling in keratinocytes. Biophysical Journal. 2017;112(11):2397-407.
20. Pasqual-Melo G, Nascimento T, Sanches LJ, Blegniski FP, Bianchi JK, Sagwal SK, et al. Plasma treatment limits cutaneous squamous cell carcinoma development in vitro and in vivo. Cancers. 2020;12(7):1993.
21. Schmidt A, Nießner F, von Woedtke T, Bekeschus S. Hyperspectral imaging of wounds reveals augmented tissue oxygenation following cold physical plasma treatment in vivo. IEEE Transactions on Radiation and Plasma Medical Sciences. 2020;5(3):412-9.
22. Arndt S, Schmidt A, Karrer S, von Woedtke T. Comparing two different plasma devices kINPen and Adtec SteriPlas regarding their molecular and cellular effects on wound healing. Clinical Plasma Medicine. 2018;9:24-33.
23. Metelmann H-R, Seebauer C, Miller V, Fridman A, Bauer G, Graves DB, et al. Clinical experience with cold plasma in the treatment of locally advanced head and neck cancer. Clinical Plasma Medicine. 2018;9:6-13.
24. Stratmann B, Costea T-C, Nolte C, Hiller J, Schmidt J, Reindel J, et al. Effect of cold atmospheric plasma therapy vs standard therapy placebo on wound healing in patients with diabetic foot ulcers: a randomized clinical trial. JAMA network open. 2020;3(7):e2010411-e.
25. Von Woedtke T, Metelmann HR, Weltmann KD. Clinical plasma medicine: state and perspectives of in vivo application of cold atmospheric plasma. Contributions to Plasma Physics. 2014;54(2):104-17.
26. Dubuc A, Monsarrat P, Virard F, Merbahi N, Sarrette J-P, Laurencin-Dalicieux S, et al. Use of cold-atmospheric plasma in oncology: A concise systematic review. Therapeutic advances in medical oncology. 2018;10:1758835918786475.
27. Hansen L, Schmidt-Bleker A, Bansemer R, Kersten H, Weltmann K-D, Reuter S. Influence of a liquid surface on the NOx production of a cold atmospheric pressure plasma jet. Journal of Physics D: Applied Physics. 2018;51(47):474002.
28. Yagi I, Ono R, Oda T, Takaki K. Two-dimensional LIF measurements of humidity and OH density resulting from evaporated water from a wet surface in plasma for medical use. Plasma Sources Science and Technology. 2014;24(1):015002.
29. Bruggeman PJ, Kushner MJ, Locke BR, Gardeniers JG, Graham W, Graves DB, et al. Plasma–liquid interactions: a review and roadmap. Plasma sources science and technology. 2016;25(5):053002.
30. Schmidt-Bleker A, Winter J, Bösel A, Reuter S, Weltmann K-D. On the plasma chemistry of a cold atmospheric argon plasma jet with shielding gas device. Plasma Sources Science and Technology. 2015;25(1):015005.
31. Schmidt-Bleker A, Winter J, Iseni S, Dünnbier M, Weltmann K, Reuter S. Reactive species output of a plasma jet with a shielding gas device—combination of FTIR absorption spectroscopy and gas phase modelling. Journal of Physics D: Applied Physics. 2014;47(14):145201.
32. Van Boxem W, Van der Paal J, Gorbanev Y, Vanuytsel S, Smits E, Dewilde S, et al. Anti-cancer capacity of plasma-treated PBS: Effect of chemical composition on cancer cell cytotoxicity. Scientific reports. 2017;7(1):16478.

33. Van Gaens W, Iseni S, Schmidt-Bleker A, Weltmann K-D, Reuter S, Bogaerts A. Numerical analysis of the effect of nitrogen and oxygen admixtures on the chemistry of an argon plasma jet operating at atmospheric pressure. New Journal of Physics. 2015;17(3):033003.
34. Reuter S, Winter J, Schmidt-Bleker A, Schroeder D, Lange H, Knake N, et al. Atomic oxygen in a cold argon plasma jet: TALIF spectroscopy in ambient air with modelling and measurements of ambient species diffusion. Plasma Sources Science and Technology. 2012;21(2):024005.
35. Schmidt-Bleker A, Norberg SA, Winter J, Johnsen E, Reuter S, Weltmann K, et al. Propagation mechanisms of guided streamers in plasma jets: the influence of electronegativity of the surrounding gas. Plasma Sources Science and Technology. 2015;24(3):035022.
36. Norberg SA, Johnsen E, Kushner MJ. Formation of reactive oxygen and nitrogen species by repetitive negatively pulsed helium atmospheric pressure plasma jets propagating into humid air. Plasma Sources Science and Technology. 2015;24(3):035026.
37. Li J, Guo H, Zhang X-F, Li H-P. Numerical and experimental studies on the interactions between the radio-frequency glow discharge plasma jet and the shielding gas at atmosphere. IEEE Transactions on Plasma Science. 2018;46(8):2766-75.
38. Lin P, Zhang J, Nguyen T, Donnelly VM, Economou DJ. Numerical simulation of an atmospheric pressure plasma jet with coaxial shielding gas. Journal of Physics D: Applied Physics. 2020;54(7):075205.
39. Semenov I, Weltmann K. Modelling of turbulent reacting flow for a cold atmospheric pressure argon plasma jet. Plasma Sources Science and Technology. 2020;29(5):055001.
40. Lindsay A, Anderson C, Slikboer E, Shannon S, Graves D. Momentum, heat, and neutral mass transport in convective atmospheric pressure plasma-liquid systems and implications for aqueous targets. Journal of Physics D: Applied Physics. 2015;48(42):424007.
41. Verlackt C, Van Boxem W, Bogaerts A. Transport and accumulation of plasma generated species in aqueous solution. Physical Chemistry Chemical Physics. 2018;20(10):6845-59.
42. Semenov I, Weltmann K, Loffhagen D. Modelling of the transport phenomena for an atmospheric-pressure plasma jet in contact with liquid. Journal of Physics D: Applied Physics. 2019;52(31):315203.
43. Heirman P, Van Boxem W, Bogaerts A. Reactivity and stability of plasma-generated oxygen and nitrogen species in buffered water solution: a computational study. Physical Chemistry Chemical Physics. 2019;21(24):12881-94.
44. Winter J, Sousa JS, Sadeghi N, Schmidt-Bleker A, Reuter S, Puech V. The spatio-temporal distribution of He (23S1) metastable atoms in a MHz-driven helium plasma jet is influenced by the oxygen/nitrogen ratio of the surrounding atmosphere. Plasma Sources Science and Technology. 2015;24(2):025015.
45. Comsol. Comsol multiphysics [Available from: www.comsol.com.
46. Van Rens JF, Schoof JT, Ummelen FC, Van Vugt DC, Bruggeman PJ, Van Veldhuizen E. Induced liquid phase flow by RF Ar cold atmospheric pressure plasma jet. IEEE Transactions on Plasma Science. 2014;42(10):2622-3.
47. Menter FR, Kuntz M, Langtry R. Ten years of industrial experience with the SST turbulence model. Turbulence, heat and mass transfer. 2003;4(1):625-32.
48. Kee RJ, Coltrin ME, Glarborg P. Chemically reacting flow: theory and practice: John Wiley & Sons; 2005.
49. Kays WM. Turbulent Prandtl number. Where are we? ASME Journal of Heat Transfer. 1994;116(2):284-95.
50. Brokaw RS. Predicting transport properties of dilute gases. Industrial & Engineering Chemistry Process Design and Development. 1969;8(2):240-53.
51. Smith GP, Golden DM, Frenklach M, Moriarty NW, Eiteneer B, Goldenberg M, et al. GRI-Mech 3.0 [Available from: www.me.berkeley.edu/gri_mech/.
52. McBride BJ. NASA Glenn coefficients for calculating thermodynamic properties of individual species: National Aeronautics and Space Administration, John H. Glenn Research Center …; 2002.

53. Stiel LI, Thodos G. The thermal conductivity of nonpolar substances in the dense gaseous and liquid regions. AIChE Journal. 1964;10(1):26-30.
54. Sander R. Compilation of Henry's law constants (version 4.0) for water as solvent. Atmospheric Chemistry and Physics. 2015;15(8):4399-981.
55. Tornin J, Labay C, Tampieri F, Ginebra M-P, Canal C. Evaluation of the effects of cold atmospheric plasma and plasma-treated liquids in cancer cell cultures. Nature Protocols. 2021;16(6):2826-50.
56. Schmidt-Bleker A, Bansemer R, Reuter S, Weltmann KD. How to produce an NOx-instead of Ox-based chemistry with a cold atmospheric plasma jet. Plasma Processes and Polymers. 2016;13(11):1120-7.
57. Reuter S, Winter J, Iséni S, Schmidt-Bleker A, Dünnbier M, Masur K, et al. The influence of feed gas humidity versus ambient humidity on atmospheric pressure plasma jet-effluent chemistry and skin cell viability. IEEE Transactions on Plasma Science. 2014;43(9):3185-92.
58. Winter J, Tresp H, Hammer M, Iseni S, Kupsch S, Schmidt-Bleker A, et al. Tracking plasma generated H2O2 from gas into liquid phase and revealing its dominant impact on human skin cells. Journal of Physics D: Applied Physics. 2014;47(28):285401.
59. Hähnel M, von Woedtke T, Weltmann KD. Influence of the air humidity on the reduction of Bacillus spores in a defined environment at atmospheric pressure using a dielectric barrier surface discharge. Plasma processes and polymers. 2010;7(3-4):244-9.
60. Mohades S, Lietz AM, Kruszelnicki J, Kushner MJ. Helium plasma jet interactions with water in well plates. Plasma Processes and Polymers. 2020;17(3):1900179.
61. Yan D, Talbot A, Nourmohammadi N, Cheng X, Canady J, Sherman J, et al. Principles of using cold atmospheric plasma stimulated media for cancer treatment. Scientific reports. 2015;5(1):18339.
62. Verreycken T, Mensink R, Van Der Horst R, Sadeghi N, Bruggeman PJ. Absolute OH density measurements in the effluent of a cold atmospheric-pressure Ar–H2O RF plasma jet in air. Plasma Sources Science and Technology. 2013;22(5):055014.
63. Gorbanev Y, Van der Paal J, Van Boxem W, Dewilde S, Bogaerts A. Reaction of chloride anion with atomic oxygen in aqueous solutions: can cold plasma help in chemistry research? Physical Chemistry Chemical Physics. 2019;21(8):4117-21.
64. Wenske S, Lackmann J-W, Busch LM, Bekeschus S, von Woedtke T, Wende K. Reactive species driven oxidative modifications of peptides—Tracing physical plasma liquid chemistry. Journal of Applied Physics. 2021;129(19).
65. Neoplas. Optional accessories for kINPen®IND [Available from: www.neoplas.eu/en/accessorieskinpenind.html.
66. Tresp H, Hammer MU, Weltmann K-D, Reuter S. Effects of atmosphere composition and liquid type on plasma-generated reactive species in biologically relevant solutions. Plasma Medicine. 2013;3(1-2).
67. Tampieri F, Gorbanev Y, Sardella E. Plasma-treated liquids in medicine: Let's get chemical. Plasma Processes and Polymers. 2023:e2300077.
68. Roquemore W, Tankin R, Chiu H, Lottes S. A study of a bluff-body combustor using laser sheet lighting. Experiments in Fluids. 1986;4:205-13.
69. Tong Y, Liu X, Chen S, Li Z, Klingmann J. Effects of the position of a bluff-body on the diffusion flames: A combined experimental and numerical study. Applied Thermal Engineering. 2018;131:507-21.
70. Kapaldo J, Han X, Ptasinska S. Shielding-gas-controlled atmospheric pressure plasma jets: Optical emission, reactive oxygen species, and the effect on cancer cells. Plasma Processes and Polymers. 2019;16(5):1800169.
71. Gazzah MH, Belmabrouk H. Directed co-flow effects on local entropy generation in turbulent heated round jets. Computers & Fluids. 2014;105:285-93.